PHILOSOPHICAL TRANSACTIONS OF THE ROYAL SOCIETY A MATHEMATICAL, PHYSICAL & ENGINEERING SCIENCES

On Nonlinear Simple Waves in Alluvial River Flows: A Theory for Sediment Bores

D. J. Needham and R. D. Hey

Phil. Trans. R. Soc. Lond. A 1991 **334**, 25-53
doi: 10.1098/rsta.1991.0002

On nonlinear simple waves in alluvial river flows: a theory for sediment bores

By D. J. Needham[1] and R. D. Hey[2]

[1] *School of Mathematics, University of East Anglia, Norwich NR4 7TJ, U.K.*
[2] *School of Environmental Sciences, University of East Anglia, Norwich NR4 7TJ, U.K.*

Contents

An increase in the upstream sediment discharge rate in an otherwise uniform alluvial flow often leads to the formation of a stable, propagating sediment bore. In this paper we study discontinuous simple wave solutions of the integral conservation laws governing flows in alluvial rivers or channels. We obtain a family of solutions, parametrized by the upstream sediment discharge rate, q_L, and the downstream Froude number, F_o, which represent stable sediment bores. It is shown that the solutions exist only in a restricted region of the (F_o, q_L) plane, and within this region, their properties are derived. A sediment bore is generated experimentally in a flume and measurements are made. The agreement between the measurements and the predictions of the theory is encouraging.

Phil. Trans. R. Soc. Lond. A (1991) **334**, 25–53
Printed in Great Britain

1. Introduction

A long-term increase in the bed-load sediment transport upstream of an otherwise uniform alluvial river flow will generally result in the formation of a large, localized step in the bedform with a planar avalanche face spanning the width of the river. This step separates the upstream flow at the higher transport rate from the downstream flow at the original, lower transport rate and propagates downstream at a speed much slower than that of the mean fluid velocity in the flow. This type of bedform is often referred to in the geophysical literature as a planar delta-form or a sediment bore and has been described by, among others, Jopling (1963, 1965, 1977) and Collinson & Thompson (1982). The term 'sediment bore' will be adopted in this paper.

A typical situation in the environment that leads to higher upstream than downstream bed-load sediment transport rates, and hence the formation and propagation of a sediment bore, occurs in rivers that experience a dramatic and sustained increase in sediment supply as, for example, where landslides suddenly inject large volumes of sediment into a river valley and this is subsequently eroded by the flow. It also occurs where nature- or man-induced disasters cause massive sediment injection to a river as, for example, a result of volcanic activity or dam bursts (see, for example, the report by Pitlick & Thorne (1987) on the Fall River in Colorado).

Further situations arising in the environment that lead to higher upstream than downstream bed-load sediment transport rates, and hence the formation and propagation of sediment bores are (*a*) river flow into a dredged section, (*b*) river flow entering a reservoir, (*c*) river flow entering an estuary.

In each of the situations (*a*)–(*c*), the flow from upstream experiences a rapid increase in depth either as it enters the dredged section or as it approaches the beginning of the reservoir or estuary basin, where the bed level is much lower than that upstream or the flow depth is increased due to back water effects. Consequently, the flow velocity downstream is much slower than that upstream, leading to a similar reduction in the downstream sediment transport rate. This situation is then as described above with a higher upstream than downstream rate of sediment transport, which invariably leads to the formation of a downstream propagating sediment bore. Observations show that the sediment bore advances via the bed load at the higher upstream transport rate 'avalanching' over the step and accumulating due to the lower downstream transport rate. In examples (*a*) and (*b*) the slowly advancing front usually has a planar structure whilst in example (*c*) the front gradually expands into the widening estuary and eventually develops curvature. With the upstream transport rate maintained, the consequences of planar sediment bore propagation in examples (*a*) and (*b*) are undesirable; in both cases, the dredged section or the reservoir will eventually be filled with sediment up to the original upstream bed level, following the passage of the sediment bore. Thus an understanding of the mechanism of sediment bore propagation is a basic management requirement in these examples. In particular, it is important to have an estimate of the propagation speed of the sediment bore to obtain timescales over which a reservoir or dredged river section will be refilled by the advancing wave front.

Particular cases of sediment bores propagating in rivers have been reported by Hasholt (1972, 1974, 1977, 1984) in detailed field surveys on three watercourses in Denmark. These studies provide a qualitative description of the propagation of a

PHILOSOPHICAL TRANSACTIONS OF THE ROYAL SOCIETY A MATHEMATICAL, PHYSICAL & ENGINEERING SCIENCES

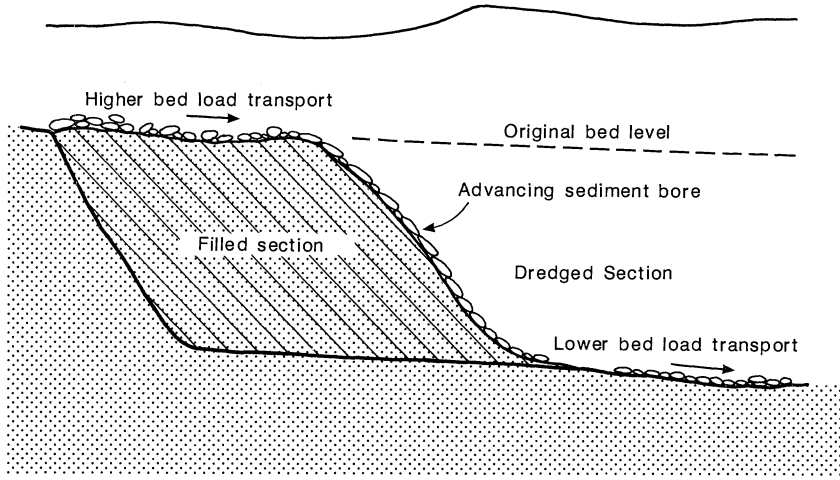

Figure 1. An illustration of an advancing sediment bore into a dredged section of a river.

sediment bore into a dredged section of river, together with the effects of re-dredging and the re-formation of the sediment bore. A further interesting description of the propagation of sediment bores into reservoirs and lakes is given by McManus (1985). This paper reports the rate of advance of a delta-form wave front into Lake Mead on the Colorado River as approximately 300 m a^{-1}, the advance of the Terek delta (on the Caspian) as approximately 300 m a^{-1}, whilst the advance of the delta form in the Lillooet River (British Columbia) is estimated at approximately 10 m a^{-1}. All of these delta forms have wave fronts with the characteristics of sediment bores. Unfortunately, further measurements are not reported. However, it is noted that the rate of progression of the wave front is dependent on the upstream water and sediment discharge rates, together with the downstream depth. To illustrate the typical situation arising in the above examples, a sketch of a sediment bore propagating into a dredged river section is shown in figure 1.

A sediment bore is readily reproduced in a laboratory flume by first maintaining a uniform alluvial flow at prescribed fluid and sediment discharge rates, after which a rapid order of magnitude increase is made in the upstream sediment discharge. The formation of a sediment bore quickly follows this increase and propagates slowly down the flume. We have been able to produce sediment bores in the flume at the University of East Anglia. A simple experiment was done by first introducing a uniform sediment (2 mm grit) input at the head of the flume and allowing the system to attain equilibrium. The sediment bore was then initiated by more than doubling the upstream rate of sediment input. A short period after the increase, a coherent sediment bore was observed to develop and propagate slowly downstream. The photograph in figure 14*a* shows the profile of the sediment bore at a time of 30 min after the initial increase in the sediment transport rate. Further details of this experiment are given in §13.

In this paper we develop a nonlinear theory to describe the propagation of a sediment bore down a straight section of an otherwise uniform alluvial river. The theory is based on the depth-averaged integral conservation laws of shallow water theory augmented by a flow resistance term, together with an integral conservation law expressing continuity of bed-load sediment, and a sediment transport function that relates the rate of bed-load sediment transport to the local mean fluid velocity.

The shallow water (or long wave) theory describes the evolution of features with a streamwise length scale much longer than the mean depth of the flow. Thus, within this framework, the sediment bore appears as a discontinuous step in the bedform separating the upstream alluvial flow with the higher bed-load transport rate from the downstream alluvial flow with the lower bed-load transport rate. The characteristics of the flow to the rear of the bedform step (that is, the flow velocity and depth, and the bed level, together with the speed of propagation of the step in bedform) are determined in terms of the flow conditions downstream and the increased upstream sediment transport rate. These large-scale features of the propagating sediment bore are thus determined by the overall conditions upstream and downstream of the wave front (that is, on upstream and downstream conditions over streamwise length scales much longer than the mean flow depth). This is exactly the situation obtained in classical fixed-bed shallow water theory where the turbulent free-surface bore is modelled as a discontinuity separating two uniform flows at differing fluid discharge rates. The detailed structure of the free-surface bore, in general a highly turbulent two-dimensional flow, does not affect, at leading order, its propagation speed or the overall conditions at distances ahead and behind the wave front. Similarly, in the present theory the detailed structure of the sediment bore wave front does not affect the overall properties considered in the paper. This structure usually consists of a locally turbulent two-dimensional flow, which is often locally two-phase, due to the turbulence lifting bed-load sediment into suspended load. As in the theory of fixed-bed turbulent bores, where the turbulence remains confined to the wave front and can be neglected in shallow-water theory, so the turbulence and suspended load local to the bed step can be neglected in the present theory, provided we are considering the flow over a streamwise length scale that is sufficiently long relative to the mean flow depth for the effects of turbulence and the quantity of suspended load sediment produced at the bed step to become negligible. This, in effect, provides a definition for the streamwise length scale in the present shallow water theory. The details of the local flow, such as turbulence, suspended load and sediment sorting, which the present theory does not aim to describe, are discussed in some detail by Jopling (1963, 1965, 1977). It is these features which account for the overall energy dissipation at the wave front of the sediment bore (as discussed in §4).

The general shallow water theory developed in this paper reveals that there are three types of simple step waves which can propagate in an alluvial river. All require an increase in the upstream sediment discharge rate. One propagates downstream with a speed comparable to that of the depth-averaged fluid velocity, but carries with it only a small step in bedform relative to the flow depth. The remaining two waves can carry larger steps in bedform. One of these waves propagates upstream, whilst the other propagates downstream. The speeds and bedform step heights vary within differing regions of the (F_o, q_L) plane, where q_L is the upstream sediment discharge rate and F_o is the downstream Froude number. In appropriately defined regions of the (F_o, q_L) plane, with $q_L > 1$, both of the latter two simple waves exhibit the characteristics of a sediment bore. A strict requirement for the downstream propagation of a sediment bore is found to be $F_o < 1$, that is the downstream uniform flow must be subcritical, which is borne out by our observations in the flume at the University of East Anglia.

PHILOSOPHICAL TRANSACTIONS OF THE ROYAL SOCIETY A MATHEMATICAL, PHYSICAL & ENGINEERING SCIENCES

2. The conservation laws

The depth-averaged hydraulic equations governing the one-dimensional flow in an alluvial river or channel are derived by considering conservation of fluid and sediment mass and fluid momentum in a section of the flow from $x = x_1$ to $x = x_2$ ($x_2 > x_1$). These three equations are then closed by the introduction of a bed-load sediment transport function. The equations, in integral conservation form, are:

$$\frac{\mathrm{d}}{\mathrm{d}t}\int_{x_1}^{x_2} h\,\mathrm{d}x + [hv]_{x_1}^{x_2} = 0, \tag{1}$$

$$\frac{\mathrm{d}}{\mathrm{d}t}\int_{x_1}^{x_2} \xi\,\mathrm{d}x - [q]_{x_1}^{x_2} = 0, \tag{2}$$

$$\frac{\mathrm{d}}{\mathrm{d}t}\int_{x_1}^{x_2} hv\,\mathrm{d}x + [v^2h + \tfrac{1}{2}gh^2]_{x_1}^{x_2} + \int_{C_{\xi_{1,2}}} gh\,\mathrm{d}y = \int_{x_1}^{x_2} R(v,h,q)\,h\,\mathrm{d}x, \tag{3}$$

$$q = G(h,v). \tag{4}$$

Here x measures distance horizontally from a fixed point 0; t is time; v is the depth-averaged horizontal fluid velocity and q is the transported bed-load sediment volume discharge rate per unit width across a vertical section. The flow depth is h and the bed level, measured vertically downwards from the x-axis, is ξ (the free surface level measured upwards from the x-axis is then $\eta = h - \xi$). The situation is illustrated in figure 2. In (3) the function $R(v,h,q)$ is the flow resistance force per unit mass whilst in (4) $G(v,h)$ is the bed-load sediment transport function. The last term on the left-hand side of (3) is a line integral with respect to y (the coordinate measuring distance vertically upwards) along the path $C_{\xi_{1,2}}$, which denotes the section of the bedform curve from $x = x_1$ to $x = x_2$. This term arises from the force in the x-direction on the fluid between $x = x_1$ and $x = x_2$ due to the normal reaction from hydrostatic pressure at the river bed. A derivation of equations (1)–(3) is given by Stoker (1957) while Cunge *et al.* (1981) discuss the effects of sediment transport associated with equation (4).

To proceed further, particular functional forms for R and G must be specified. For R we use the Chézy law (see, for example, Gibson 1934), which for a wide channel of rectangular section may be written as,

$$R = -\tilde{\mathscr{C}}_{\mathrm{f}}(q)\,v^2/h. \tag{5}$$

This allows for the dimensionless Chézy coefficient $\tilde{\mathscr{C}}_{\mathrm{f}}$ to depend on the local rate of bed-load sediment transport, q, through

$$\tilde{\mathscr{C}}_{\mathrm{f}} = \mathscr{C}_{\mathrm{f}}/(1 + \mathscr{C}_{\mathrm{s}}\,q), \tag{6}$$

where $\mathscr{C}_{\mathrm{f}}$ is the usual Chézy coefficient for the flow in the absence of bed-load sediment transport and $\mathscr{C}_{\mathrm{s}}$ is a material constant measuring the magnitude of the influence of sediment transport on flow resistance. This simple form for $\tilde{\mathscr{C}}_{\mathrm{f}}$ allows for a reduction in flow resistance with increasing bed-load sediment transport provided the bed remains plane. Although we have proposed a detailed form for the flow resistance, R, in (6), we shall see that the equations derived from (1)–(4) which relate conditions immediately upstream and downstream of a discontinuous wavefront do not, in fact, involve R. This is to be expected, since R appears in equation (3) as a body force.

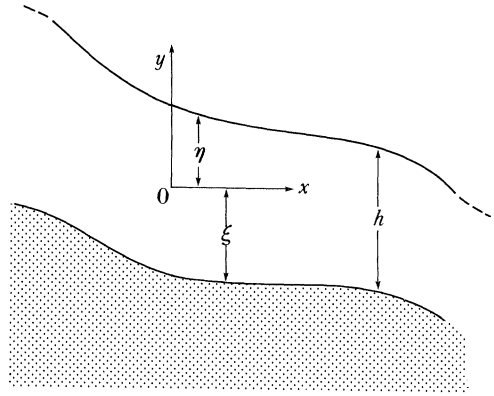

Figure 2. A sketch of the coordinate system.

For G we follow Cunge *et al.* (1981), and use the simple form,

$$G = mv^n, \tag{7}$$

where m will, in general, depend upon the flow characteristics and n is constant. In many practical situations it has been demonstrated, at least for slowly varying alluvial flows, that $1 \leqslant n \leqslant 2$. However, larger values of n may be attained when the bed is dune covered, Engelund & Hansen (1967). Many of the available sediment transport functions are reasonably well approximated by taking m as constant in (7). For simplicity we adopt this approximation in the present paper, and also take $n = 2$. It is expected that these approximations will be at least qualitatively, if not always quantitatively, accurate over a reasonably wide range of flow situations. Moreover, it is readily observed in performing the analysis that the qualitative nature of the results obtained in this paper are unchanged with differing functional forms for G, provided it remains as a positive, monotone increasing function of $v(> 0)$.

Observations of sediment bores in both natural water courses and in flumes (see figure 14*a*) indicate that the horizontal length scale over which the step in bedform takes place is comparable with the overall flow depth. This suggests that in terms of the shallow water theory description of alluvial river flows (as represented by equations (1)–(4)) the local structure of the sediment bore will be unresolved, and the bore wave front will appear as a simple step discontinuity in the bedform. Therefore, if the shallow water theory is to be adequate for describing sediment bore propagation, we will require equations (1)–(4) to admit solutions which contain simple step discontinuities in h, v, q and ξ, as illustrated in figure 3, where the discontinuity is positioned at $x = s(t)$, with conditions immediately upstream and downstream of the discontinuity referred to by subscripts L and R respectively. Equations (1), (2) and (4) certainly allow solutions that have simple step discontinuities in h, v, q and ξ. However, equation (3) requires more careful consideration. Although the first two terms on the left-hand side together with the last term on the right-hand side of equation (3) admit simple step discontinuities in h, v, and q, it remains to examine the last term on the left-hand side, namely,

$$\int_{C_{\xi_{1,2}}} gh \, \mathrm{d}y. \tag{8}$$

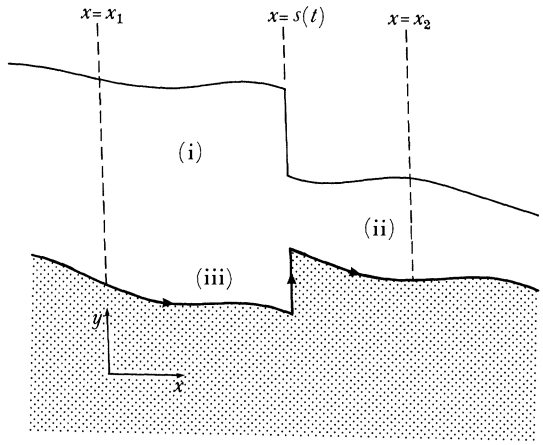

Figure 3. A simple jump discontinuity located at $x = s(t)$ illustrating the notation of §3. Upstream of the discontinuity (i), conditions h_{L}, ξ_{L}, V_{L}; downstream of the discontinuity (ii), conditions h_{R}, V_{R}, ξ_{R}. The path of the line integral (iii), is $C_{\xi_{1,2}}$.

With x_1, x_2 either side of the discontinuity, the path, $C_{\xi_{1,2}}$, of the line integral (8) remains well defined, as illustrated in figure 3. However, the line integral (8) cannot be evaluated along that section of the path $C_{\xi_{1,2}}$ which constitutes the face of the step in bedform. This is because the function h in the integrand of (8) is, in general, not well defined along the face. At any point on the face, h measures the vertical distance between this point and the free surface of the water. However, since the free surface of the water will, in general, be simultaneously discontinuous, h cannot be resolved along the face of the step in bedform. We must conclude that equations (1)–(4) cannot admit solutions with simple step discontinuities in h, v, q and ξ. To allow the possibility of discontinuous solutions, the model of the flow provided by equations (1)–(4) must be extended to include a definition of h (as a function of y) along the face of a step in bedform; that is, we must include information concerning the structure of the sediment bore over a horizontal length scale comparable with the flow depth. To this end we augment the flow description provided by equations (1)–(4) with the condition that along the face of a step discontinuity in bedform,

$$h = d'(y), \quad \min\{-\xi_{\mathrm{L}}, -\xi_{\mathrm{R}}\} < y < \max\{-\xi_{\mathrm{L}}, -\xi_{\mathrm{R}}\}, \tag{9}$$

where $d'(\cdot)$ is a positive differentiable function in its interval of definition and satisfies the end conditions,

$$d'(-\xi_{\mathrm{L}}) = h_{\mathrm{L}}, \quad d'(-\xi_{\mathrm{R}}) = h_{\mathrm{R}}. \tag{10}$$

In addition it is reasonable to require that $d'(y)$ is a monotone function of y. The inclusion of a specific form for $d'(y)$ is somewhat arbitrary, up to the conditions specified above. However, since $d'(y)$ models the depth–bedform relation across the thin wave front, we expect that the overall conclusions from the theory (qualitatively at least) will not be strongly sensitive to changes in the details of $d'(y)$.

An alternative approach would be to extend the present model by including higher order effects in equations (3) and (4); for example, the inclusion of the term $[-\nu(v, h)\,\partial v/\partial x]_{x_1}^{x_2}$ on the left-hand side of (3) (representing a longitudinal stress in the fluid, with ν an appropriately defined Eddy viscosity), together with a higher-order description of the momentum balance in bed-load sediment transport in (4). The

inclusion of such terms would resolve the structure of discontinuities and provide a function $d'(y)$ (as the variation in depth with bedform elevation throughout the structure) to augment the lower-order theory; equations (1)–(4). However, it is not clear at present how the model provided by equations (1)–(4) could be rationally extended to higher order, without making those equations considerably more complex. We therefore adopt the former approach of augmenting equations (1)–(4) with condition (9). The proposal of a specific form for $d'(y)$ is considered at a later stage.

With a constant fluid discharge Q_o and sediment discharge q_o the most simple solution of equations (1)–(7) is that representing a uniform flow down an incline of slope S, where $h = h_o$, $v = v_o$ are constants and $\xi = Sx$. After substitution into equations (1)–(7) we obtain the following expressions,

$$v_o = \left[\frac{q_o}{m}\right]^{\frac{1}{2}}, \quad h_o = \left[\frac{Q_o^2 m}{q_o}\right]^{\frac{1}{2}}, \quad S = \frac{\mathscr{C}_f}{gQ_o(1+\mathscr{C}_s q_o)}\left[\frac{q_o}{m}\right]^{\frac{3}{2}}, \tag{11}$$

which determine the flow speed, depth and slope for the uniform flow in terms of Q_o, q_o and the material parameters $\mathscr{C}_f$, $\mathscr{C}_s$ and m.

Henceforth we consider the propagation of simple waves into the uniform flow, generated by a change in the upstream sediment discharge. Thus typical scales for the fluid velocity, depth and sediment discharge are v_o, h_o and q_o respectively. In general, there will also be a characteristic timescale, say t_o, associated with the flow, which leads to a characteristic length scale given by $l_o = v_o t_o$. We use these scales to introduce the following dimensionless variables:

$$v = v_o\, v', \quad h = h_o\, h', \quad \xi = h_o\, \xi', \quad q = q_o\, q', \quad y = h_o\, y', \quad x = l_o\, x', \quad t = t_o\, t'. \tag{12}$$

After dispensing with primes for convenience, equations (1)–(7) become, in dimensionless form:

$$\frac{\mathrm{d}}{\mathrm{d}t}\int_{x_1}^{x_2} h\,\mathrm{d}x + [hv]_{x_1}^{x_2} = 0, \tag{13a}$$

$$\frac{\mathrm{d}}{\mathrm{d}t}\int_{x_1}^{x_2} \xi\,\mathrm{d}x - \epsilon[v^2]_{x_1}^{x_2} = 0, \tag{13b}$$

$$\frac{\mathrm{d}}{\mathrm{d}t}\int_{x_1}^{x_2} hv\,\mathrm{d}x + \left[v^2 h + \frac{1}{2F_o^2}h^2\right]_{x_1}^{x_2} + \frac{1}{F_o^2}\int_{C_{\xi_{1,2}}} h\,\mathrm{d}y = -\frac{1}{\sigma}\int_{x_1}^{x_2}\frac{v^2}{(1+\theta v^2)}\,\mathrm{d}x, \tag{13c}$$

$$q = v^2, \tag{13d}$$

where q has been replaced from (4), via (7) in (3), and R has been replaced from (5) into (3). Equation (13a–c) now serve to determine h, v and ξ, after which q is obtained from (13d). Four dimensionless parameters have been introduced in (13a–c). $F_o = v_o/\sqrt{(gh_o)}$ is the Froude number of the uniform flow, whilst $\epsilon = q_o/Q_o$ measures the overall ratio of sediment to fluid discharge in the flow and $\sigma = h_o/t_o\, v_o\, \mathscr{C}_f$ gives a dimensionless measure of the inverse timescale associated with the flow. Also, $\theta = \mathscr{C}_s\, q_o$ provides a dimensionless measure of the effect of bed-load sediment transport on flow resistance. It should be noted that in the limit $\epsilon, \theta \to 0$, equation (13a–c) reduce to those of fixed-bed hydraulics, while allowing $\theta \to 0$ alone decouples flow resistance from the effects of sediment transport.

In terms of the dimensionless variables the uniform flow becomes,

$$v = 1, \quad h = 1, \quad \xi = F_0^2/\sigma(1+\theta)\, x, \quad q = 1. \tag{14}$$

We now consider the conditions which must be satisfied across a simple step discontinuity which may occur in the solutions of equation (13*a–c*), when augmented with condition (9) (in a suitable dimensionless form).

3. Conditions at a step discontinuity

As discussed in §2, the integral conservation laws (13*a–c*), when augmented with condition (9), may admit solutions that contain simple step discontinuities in h, v and ξ. Here we obtain the appropriate forms for the jumps in h, v and ξ across such a discontinuity.

We suppose that a solution of (13*a–c*) has a simple step discontinuity at position $x = s(t)$ across which condition (9) holds, with h, v, ξ continuous and differentiable on either side of the discontinuity. The fixed stations x_1 and x_2 are chosen so that $x_1 < s(t) < x_2$, and we denote variables upstream ($x - s(t) < 0$) and downstream ($x - s(t) > 0$) by the subscripts L and R respectively. The situation is illustrated in figure 3. The notation $[\,\cdot\,]_{\mathrm{L}}^{\mathrm{R}}$ denotes the downstream to upstream difference across the discontinuity.

To derive the jump conditions, we split the range of integration in (13*a–c*) by writing

$$\int_{x_1}^{x_2} \quad \text{as} \quad \int_{x_1}^{s(t)} + \int_{s(t)}^{x_2},$$

after which the limit $x_1, x_2 \to s(t)$ is taken. The jump conditions corresponding to equation (13*a*, *b*) are readily obtained as

$$[h(v-\dot{s})]_{\mathrm{L}}^{\mathrm{R}} = 0, \tag{15a}$$

$$[\epsilon v^2 + \xi\dot{s}]_{\mathrm{L}}^{\mathrm{R}} = 0, \tag{15b}$$

whilst the jump condition associated with equation (13*c*) requires,

$$[hv\dot{s} - v^2 h - h^2/2F_0^2 - (1/F_0^2)\,\mathrm{d}(-\xi)]_{\mathrm{L}}^{\mathrm{R}} = 0, \tag{15c}$$

after using (9) to evaluate the line integral along the face of the step in bedform.

The conditions (15*a–c*) must be satisfied across any discontinuity that develops in a solution of equation (13*a–c*). It should be noted that in the limit $\epsilon \to 0$ with $[\xi]_{\mathrm{L}}^{\mathrm{R}} = 0$, conditions (15*a–c*) reduce to the usual jump conditions required at a discontinuity in fixed-bed hydraulics. In addition, it is important to note that the jump condition (15*c*) is uninfluenced by the body force term on the right side of equation (13*c*). In particular, this means that the jump conditions are independent of the nature of the flow resistance term and of the parameter σ, which measures the ratio of the order of magnitude of the inertia and pressure gradient terms to that of the body force terms. In fact the only dimensionless parameters appearing in the jump conditions are the Froude number F_0 and ϵ.

We next consider the dissipation of kinetic and gravitational potential energy in the flow due to the presence of a discontinuity.

4. Energy dissipation at a discontinuity

We consider again the section of the flow between $x = x_1$ and $x = x_2$, as illustrated in figure 3. Within this section a consideration of the rate of dissipation of mechanical energy in the flow leads to the expression

$$\frac{\mathrm{d}D}{\mathrm{d}t} = \tfrac{1}{2}[hv^3]_{\mathrm{R}}^{\mathrm{L}} - \tfrac{1}{2}\,\dot{s}\,[hv^2]_{\mathrm{R}}^{\mathrm{L}} - \frac{1}{F_{\mathrm{o}}^2}[(h-\xi)\,vh]_{\mathrm{R}}^{\mathrm{L}} - \frac{\dot{s}}{2F_{\mathrm{o}}^2}[(\xi-h)^2-(\xi)^2]_{\mathrm{R}}^{\mathrm{L}} + \frac{\dot{s}}{F_{\mathrm{o}}^2}[d(-\xi)]_{\mathrm{R}}^{\mathrm{L}}. \quad (16)$$

Here $\mathrm{d}D/\mathrm{d}t$ is the rate of energy dissipation at the discontinuity, which has been made dimensionless with $\rho h_{\mathrm{o}}\, v_{\mathrm{o}}{}^3$. The only term in (16) which does not arise in fixed-bed hydraulics is the final term which represents the rate of working of the normal reaction at the bed step. On physical grounds, any discontinuity in a solution of equation (13*a–c*) with condition (9) cannot create energy. Thus we require

$$\mathrm{d}D/\mathrm{d}t \geqslant 0 \quad (17)$$

at a discontinuity.

5. Contact discontinuities

Before examining simple wave solutions in detail we first consider whether discontinuities are possible, across which one or more of the variables remain continuous. This type of discontinuity is often referred to as a contact discontinuity.

On using the conditions (15*a–c*) it is readily shown that the only possible contact discontinuity has h and v continuous with $\dot{s} = 0$, after which (15*c*) reduces to $d(-\xi_{\mathrm{L}}) = d(-\xi_{\mathrm{R}})$. However,

$$d(-\xi_{\mathrm{L}}) - d(-\xi_{\mathrm{R}}) = \int_{y=-\xi_{\mathrm{R}}}^{y=-\xi_{\mathrm{L}}} d'(y)\,\mathrm{d}y,$$

which cannot vanish (since $d'(y) > 0$) unless $\xi_{\mathrm{L}} = \xi_{\mathrm{R}}$, and all variables are then continuous. Thus at a point of discontinuity, h, v and ξ are all required to be discontinuous and contact discontinuities are not possible.

6. A functional form for $d'(y)$

To consider simple waves in detail we must first specify a functional form for $d'(y)$. We take the most simple form, in which $d'(y)$ is a linear function of y. On satisfying conditions (10), we obtain

$$d'(y) = h_{\mathrm{L}} - (\xi_{\mathrm{L}}+y)\,(\xi_{\mathrm{L}}-\xi_{\mathrm{R}})^{-1}\,(h_{\mathrm{L}}-h_{\mathrm{R}}), \quad \min\{-\xi_{\mathrm{L}},-\xi_{\mathrm{R}}\} \leqslant y \leqslant \max\{-\xi_{\mathrm{L}},-\xi_{\mathrm{R}}\}. \quad (18)$$

Although this choice is somewhat arbitrary, observations of the structure across a sediment bore wave front (see, for example, figure 14*a*) show that the flow depth changes almost linearly with the bedform elevation, which lends quantitative support to our chosen form for $d'(y)$ in (18).

The function $d(y)$ is obtained directly from (18), via integration, as

$$d(y) = h_{\mathrm{L}}\,y - \tfrac{1}{2}y(2\xi_{\mathrm{L}}+y)\,(\xi_{\mathrm{L}}-\xi_{\mathrm{R}})^{-1}\,(h_{\mathrm{L}}-h_{\mathrm{R}}),$$
$$\min\{-\xi_{\mathrm{L}},-\xi_{\mathrm{R}}\} \leqslant y \leqslant \min\{-\xi_{\mathrm{L}},-\xi_{\mathrm{R}}\}. \quad (19a)$$

The constant of integration is neglected since d appears only as a difference in equations (15*c*) and (16). On using (19*a*) we find, after some algebra, that

$$[d(-\xi)]_{\mathrm{R}}^{\mathrm{L}} = \tfrac{1}{2}(\xi_{\mathrm{R}}-\xi_{\mathrm{L}})\,(h_{\mathrm{R}}+h_{\mathrm{L}}). \quad (19b)$$

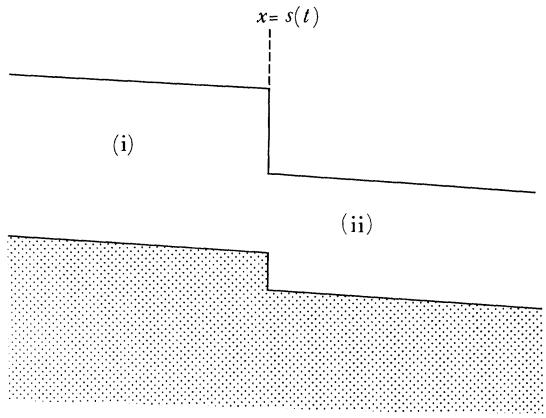

Figure 4. A sketch of the simple wave solution. At (i) $\bar{\xi} = \bar{\xi}_{\mathrm{L}}$, $h = h_{\mathrm{L}} = H$, $V = V_{\mathrm{L}}$; at (ii) $\bar{\xi} = 0$, $h = 1$, $V = 1$.

7. Simple wave solutions

In this section we examine a family of simple wave solutions of equations (13*a–c*). These solutions are generated by a change in upstream conditions in an otherwise uniform alluvial flow. The change in conditions generates a discontinuity which then propagates into the original downstream uniform flow. Since we are considering a discontinuity propagating into the uniform flow (14), it is first convenient to write

$$\xi = F_{\mathrm{o}}^2\, x/\sigma(1+\theta) - \bar{\xi} \tag{20a}$$

and work with $\bar{\xi}$ (which measures the upward displacement of the bedform from the line $y = -F_{\mathrm{o}}^2\, x/\sigma(1+\theta)$) rather than ξ. Thus to the right of the discontinuity (downstream) we have the uniform flow, so that, using (14) and (20*a*)

$$v = v_{\mathrm{R}} = 1, \quad h = h_{\mathrm{R}} = 1, \quad \bar{\xi} = \bar{\xi}_{\mathrm{R}} = 0. \tag{20b}$$

To the left (upstream) of the discontinuity a modified flow is generated by a prescribed change in the sediment discharge rate. The simplest upstream flow which may be obtained by a change in the upstream sediment discharge rate is the modified uniform flow corresponding to the altered sediment discharge rate. It is this situation that we pursue in the present paper. However, for non-uniform steady flow conditions upstream of the discontinuity, the following theory remains valid, with v_{L}, H and $\bar{\xi}_{\mathrm{L}}$ (as obtained below), then providing downstream boundary conditions for the non-uniform steady upstream flow.

Thus to the left of the discontinuity we consider a modified uniform flow at the altered sediment discharge rate. In this situation the flow will be steady in a frame of reference moving with the propagation speed of the discontinuity, and no natural timescale is present in the flow. Therefore in what follows we may set, without loss of generality, $t_{\mathrm{o}} = h_{\mathrm{o}}/v_{\mathrm{o}}\mathscr{C}_{\mathrm{f}}$ after which $\sigma = 1$.

To proceed it is convenient, for the present, to think of the modified uniform flow upstream of the discontinuity as being generated by a given depth change $h = h_{\mathrm{L}} = H$. With the discontinuity at $x = s(t)$, the flow to the left (upstream) is then given by, from equations (13*a–c*),

$$v = v_{\mathrm{L}}, \quad h = h_{\mathrm{L}} = H, \quad \bar{\xi} = \frac{1}{(1+\theta)}\left\{F_{\mathrm{o}}^2 - \frac{(1+\theta)\,F_{\mathrm{L}}^2}{(1+\theta v_{\mathrm{L}}^2)}\right\}(x - s(t)) + \bar{\xi}_{\mathrm{L}}, \tag{21}$$

PHILOSOPHICAL TRANSACTIONS OF THE ROYAL SOCIETY A MATHEMATICAL, PHYSICAL & ENGINEERING SCIENCES

where $F_L = F_o\, v_L/H^{\frac{1}{2}}$ is the upstream Froude number and the constants v_L and $\bar{\xi}_L$ are to be determined. A schematic representation of the simple wave is shown in figure 4.

The jump conditions (15*a–c*) provide three equations to be solved for the three unknowns v_L, $\bar{\xi}_L$ and $\dot{s}(t)$ as functions of the two parameters F_o and H. It is convenient to write conditions (15*a–c*) in terms of a frame of reference relative to the moving discontinuity. Thus we introduce

$$\hat{v}_L = v_L - \dot{s}(t), \tag{22}$$

where $\hat{v}_L$ is the fluid velocity on the left relative to the moving discontinuity. In terms of $\hat{v}_L$, conditions (15*a–c*) become, after use of (19*b*)–(22),

$$H\hat{v}_L = (1-\dot{s}), \tag{23a}$$

$$\epsilon(\hat{v}_L+\dot{s})^2 - \bar{\xi}_L\,\dot{s} = \epsilon, \tag{23b}$$

$$(1-\dot{s})\,[(1-\dot{s})-\hat{v}_L] - \tfrac{1}{2}F_o^{-2}\,(H^2-1) = \tfrac{1}{2}F_o^{-2}\,(H+1)\,\bar{\xi}_L. \tag{23c}$$

We first solve (23*a*, *b*) for $\hat{v}_L$ and $\bar{\xi}_L$ to obtain,

$$\hat{v}_L = (1-\dot{s})/H, \tag{24a}$$

$$\bar{\xi}_L = \epsilon(1-\dot{s})\,(1-H)\,[(1+H)-\dot{s}(1-H)]/\dot{s}H^2. \tag{24b}$$

The above expressions are now used to eliminate $\hat{v}_L$ and $\bar{\xi}_L$ from (23*c*) which leads to a single cubic equation to be solved for $\dot{s}$ as a function of the parameters ϵ, H and F_o, namely,

$$\dot{s}^3 + \frac{1}{2F_o^2}\left\{\epsilon\frac{(1-H^2)}{H} - 4F_o^2\right\}\dot{s}^2 + \frac{1}{2F_o^2}\left\{2F_o^2 - (H+1)\,H - 2\epsilon\frac{(H+1)}{H}\right\}\dot{s} + \frac{\epsilon(H+1)^2}{2F_o^2\,H} = 0. \tag{25}$$

As a check, we note that as $H \to 1$ the three roots of equation (25) reduce to the three linearized dynamic wave speeds for small disturbances to the uniform flow, as given by Needham (1990). We now consider the solutions of equation (25) when $\epsilon \ll 1$, a condition which is satisfied in practice by the majority of alluvial river flows. We use singular perturbation theory (see, for example, Nayfeh 1981) to develop the asymptotics of the roots directly from equation (25). This approach is adopted as it clearly unfolds the nature of the perturbation $0 < \epsilon \ll 1$ for mobile-bed hydraulics from the case $\epsilon = 0$ for fixed-bed hydraulics.

8. The theory for $\epsilon \ll 1$

We consider the solution of equation (25) for $\epsilon \ll 1$. An examination of (25) shows that as $\epsilon \to 0$, two of the roots are of $O(1)$, whilst the other is of $O(\epsilon)$. We consider first the two roots which are of $O(1)$ as $\epsilon \to 0$.

8.1. *The $O(1)$ roots*

With $\dot{s}$ of $O(1)$ as $\epsilon \to 0$ equation (25) reduces to a quadratic equation at leading order, with roots,

$$\dot{s} = \dot{s}_\pm \sim 1 \pm \sqrt{(H(H+1)/2F_o^2)} \quad \text{as} \quad \epsilon \to 0, \tag{26}$$

with '+' and '−' referring to the upper and lower root respectively. These are the usual speeds obtained in fixed-bed hydraulics for the propagation of a hydraulic jump of depth H into a uniform flow of Froude number F_o.

We now consider the energy dissipated at a discontinuity with speed $\dot{s}_{\pm}$. With $\dot{s}$ of $O(1)$, we see from (24*b*) that $\bar{\xi}_{\mathrm{L}}$ is of $O(\epsilon)$. Thus, at leading order, the rate of energy dissipation becomes, via (16), (19*b*), (22) and (23*a*–*c*),

$$\mathrm{d}D/\mathrm{d}t \sim (1-\dot{s})\,(1-H)^3/4F_{\mathrm{o}}^2\,H; \quad \epsilon \to 0, \quad \dot{s} = O(1). \tag{27}$$

$\dot{s} = \dot{s}_+$

For the family of discontinuous solutions with $\dot{s} = \dot{s}_+$, we have $(1-\dot{s}_+) < 0$ for all H, $F_{\mathrm{o}} > 0$. The requirement (17), that energy should be dissipated at the discontinuity, then reduces to, via (27), $H > 1$. Thus, in the positive quadrant of the (H, F_{o}) plane, the family of discontinuous solutions with speed $\dot{s}_+$ exist only in the domain

$$D_+ = \{(H, F_{\mathrm{o}}) : H > 1,\, F_{\mathrm{o}} > 0\}. \tag{28}$$

This family of solutions move downstream with a speed greater than unity, carrying with them an increase in upstream flow depth.

$\dot{s} = \dot{s}_-$

For this family of discontinuous solutions we have $(1-\dot{s}_-) > 0$ for F_{o}, $H > 0$, and energy dissipation requires, via (27), that $0 < H < 1$. Therefore, this family of discontinuous solutions, with speed $\dot{s}_-$, exists only in the domain

$$D_- = \{(H, F_{\mathrm{o}}) : 0 < H < 1,\, F_{\mathrm{o}} > 0\}, \tag{29}$$

of the (H, F_{o}) plane. An examination of (26) shows that

$$\dot{s}_- \begin{cases} > 0; & G(H, F_{\mathrm{o}}) < 0, \\ < 0; & G(H, F_{\mathrm{o}}) > 0, \end{cases} \tag{30a}$$

where

$$G(H, F_{\mathrm{o}}) \equiv H(H+1) - 2F_{\mathrm{o}}^2. \tag{30b}$$

Thus an $\dot{s}_-$ discontinuity may propagate either upstream or downstream depending upon the sign of $G(H, F_{\mathrm{o}})$ in D_-. In both cases the discontinuity carries a decrease in upstream flow depth.

For both of the $\dot{s}_{\pm}$ family of solutions, the associated jumps in v and $\bar{\xi}$ are obtained from (24*a*, *b*) as

$$[v_{\pm}]_{\mathrm{R}}^{\mathrm{L}} = [\hat{v}_{\pm}]_{\mathrm{R}}^{\mathrm{L}} \sim \pm[(H-1)/H]\,(H(H+1)/2F_{\mathrm{o}}^2)^{\frac{1}{2}} > 0, \tag{31a}$$

$$[\bar{\xi}_{\pm}]_{\mathrm{R}}^{\mathrm{L}} = \bar{\xi}_{\mathrm{L}} \sim \frac{\pm\epsilon(H-1)\,(H(H+1))^{\frac{1}{2}}\{2 \pm ((H-1)/H)\,(H(H+1)/2F_{\mathrm{o}}^2)^{\frac{1}{2}}\}}{\sqrt{(2F_{\mathrm{o}}^2)}\,H(1 \pm (H(H+1)/2F_{\mathrm{o}}^2)^{\frac{1}{2}})} \begin{cases} > 0; \dot{s}_+, & \\ > 0; \dot{s}_-, & G < 0, \\ < 0; \dot{s}_-, & G > 0, \end{cases} \tag{31b}$$

and the relative upstream and downstream Froude numbers are

$$F_{\mathrm{L}} \sim ((H+1)/2H^2)^{\frac{1}{2}} \begin{cases} < 1, \dot{s}_+, \\ > 1, \dot{s}_-, \end{cases} \quad F_{\mathrm{R}} \sim (H(H+1)/2)^{\frac{1}{2}} \begin{cases} > 1, \dot{s}_+, \\ < 1, \dot{s}_-. \end{cases}$$

We see from (31*b*) that discontinuous solutions in the $\dot{s}_{\pm}$ families carry only a small step in bedform of $O(\epsilon)$. An illustration of a typical $\dot{s}_+$ solution is shown in figure 5(*a*), while illustrations of $\dot{s}_-$ solutions are shown in figure 5*b*, *c* for $\dot{s}_- \lessgtr 0$ respectively.

This completes the details of the two families of discontinuous solutions with speeds $\dot{s}_{\pm}$. Both families exist in complementary regions of the (H, F_{o}) plane, namely D_+ and D_-. Both have speeds of $O(1)$ but carry only an $O(\epsilon)$ step in bedform. These two families do not have the characteristics of the slow moving sediment bore which

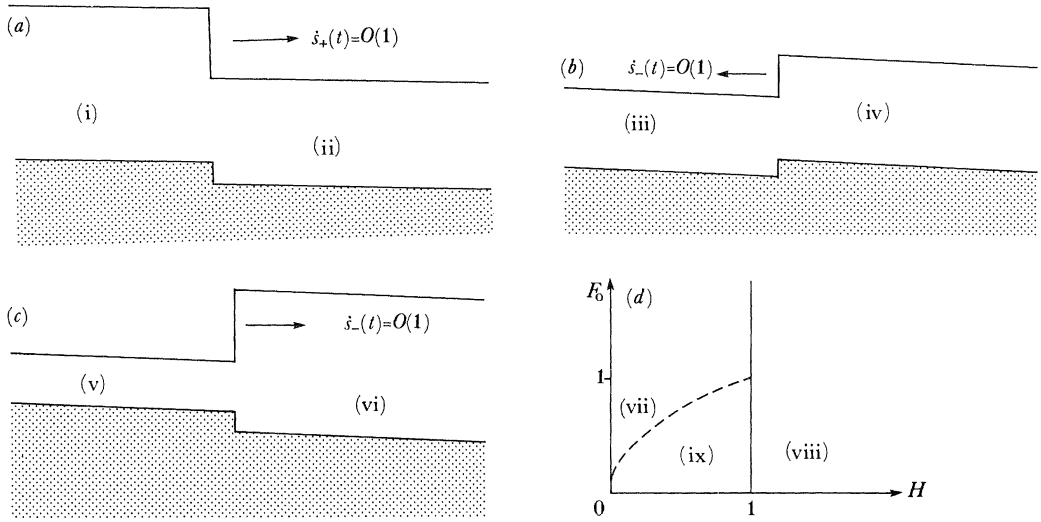

Figure 5. (*a*) The simple wave solution with $\dot{s} = \dot{s}_+$. At (i): $h = H > 1$, $V = V_L > 1$, $\bar{\xi}_L = O(\epsilon)$. At (ii): $V = h = 1$, $\bar{\xi} = 0$. (*b*) The simple wave solution with $\dot{s} = \dot{s}_- < 0$. At (iii): $h = H < 1$, $V = V_L > 1$, $\bar{\xi}_L = O(\epsilon)$. At (iv): $V = h = 1$, $\bar{\xi} = 0$. (*c*) The simple wave solution with $\dot{s} = \dot{s}_- > 0$. At (v): $h = H < 1$, $V = V_L > 1$, $\bar{\xi}_L = O(\epsilon)$. At (vi): $V = h = 1$, $\bar{\xi} = 0$. (*d*) The domain of existance of the $\dot{s}_\pm$ waves in the (H, F_o) plane. At (vii): D_-, $0 < \dot{s}_- < 1$, $\bar{\xi}_L > 0$. At (viii): D_+, $\dot{s}_+ > 1$, $\bar{\xi}_L > 0$. At (ix): D_-, $\dot{s}_- < 0$, $\bar{\xi}_L < 0$.

carries an $O(1)$ step in bedform. In fact the D_+ families are primarily river waves, reducing, in the limit $\epsilon \to 0$, to the usual turbulent bores of fixed-bed hydraulics. The domains in which these solutions exist, $D_\pm$, are illustrated on the (H, F_o) plane in figure 5*d*.

We next consider the solution corresponding to the remaining root of equation (25).

8.2. *The $O(\epsilon)$ root*

The remaining root of equation (25) is of $O(\epsilon)$ as $\epsilon \to 0$. Thus we put

$$\dot{s} = \epsilon\omega, \tag{32}$$

with ω of $O(1)$. After writing (25) in terms of ω, we obtain at leading order,

$$\{2F_o^2 - H(H+1)\}\,\omega + (H+1)^2/H + O(\epsilon) = 0, \tag{33}$$

which has the single root $\omega = (H+1)^2/HG(H, F_o)$. Therefore, in this case, we have a single family of solutions which propagate with the slow speed, from above,

$$\dot{s} = \dot{s}_b \sim \epsilon(H+1)^2/HG(H, F_o). \tag{34}$$

We now consider the domain of existence of this family of solutions in the positive quadrant of the (H, F_o) plane. First, we observe from (34) that $\dot{s}_b$ changes sign across the curve $G(H, F_o) = 0$, with $\dot{s}_b > 0$ in R_{b+} and $\dot{s}_b < 0$ in R_{b-}, where,

$$R_{b+} = \{(H, F_o)\colon H > 0,\ 0 < F_o < \tfrac{1}{\sqrt{2}}\sqrt{(H(H+1))}\}, \tag{35a}$$

$$R_{b-} = \{(H, F_o)\colon H > 0,\ F_o > \tfrac{1}{\sqrt{2}}\sqrt{(H(H+1))}\}. \tag{35b}$$

Also, with $\dot{s}$ of $O(\epsilon)$, equation (24*a*, *b*) reduces to,

$$v_L \sim \hat{v}_L \sim 1/H, \quad \bar{\xi}_L \sim \epsilon(1-H^2)/\dot{s}_b H^2. \tag{36a, b}$$

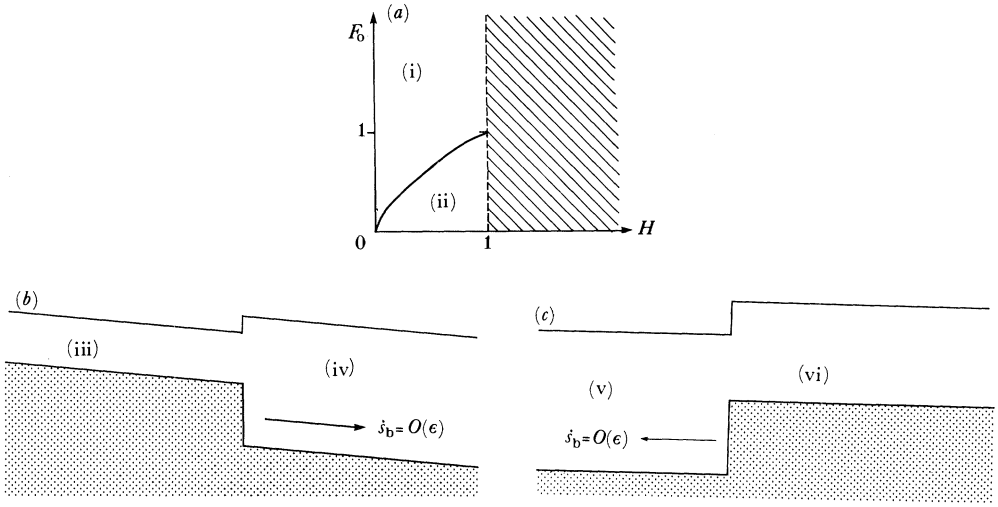

Figure 6. (*a*) The region $R_{b\pm}$ in the (H, F_o) plane. At (i): $\dot{s}_b < 0$, $\bar{\xi}_L < 0$. At (ii): $\dot{s}_b > 0$, $\bar{\xi}_L > 0$. (*b*) The simple wave solution with $\dot{s} = \dot{s}_b > 0$. At (iii): $V = V_L > 1$, $h = H < 1$, $\bar{\xi}_L = O(1)$. At (iv): $V = h = 1$, $\bar{\xi} = 0$. (*c*) The simple wave solution with $\dot{s} = \dot{s}_b < 0$. At (v): $V = V_L > 1$, $h = H < 1$, $\bar{\xi}_L = O(1)$. At (vi): $V = h = 1$, $\bar{\xi} = 0$.

Finally we must consider energy dissipation at the discontinuity. With $\dot{s}$ of $O(\epsilon)$ and $\bar{\xi}_L$ of $O(1)$, equation (16) reduces to, at leading order,

$$\mathrm{d}D/\mathrm{d}t \sim ((1-H)/2H(1+H))\,(1+6H+H^2), \tag{37}$$

where v_L and $\bar{\xi}_L$ have been replaced using (36*a*, *b*). An examination of (37) shows that energy is dissipated by this family of solutions $((\mathrm{d}D/\mathrm{d}t) > 0)$ if and only if, $0 < H < 1$. Therefore these simple waves exist only in the domain D_b of the positive quadrant of the (H, F_o) plane, where,

$$D_b = \{(H, F_o)\colon 0 < H < 1,\ F_o > 0\}. \tag{38}$$

The associated jumps in v and $\bar{\xi}$ are calculated from (36*a*, *b*) as,

$$[v_b]_R^L = [\hat{v}_b]_R^L \sim \frac{1}{H} - 1 > 0, \tag{39a}$$

$$[\bar{\xi}_b]_R^L = \bar{\xi}_L \sim (1-H)\,G(H, F_o)/((H+1)\,H). \tag{39b}$$

To summarize, we observe that this family of simple waves exists in D_b. In $D_b \cap R_{b+}$ the wave propagates slowly downstream with a speed of $O(\epsilon)$, accompanied by an $O(1)$ downstream facing step in bedform, and a decrease in upstream flow depth. In the complementary region $D_b \cap R_{b-}$ the simple wave propagates slowly upstream with a speed of $O(\epsilon)$, accompanied by an $O(1)$ upstream facing step in bedform and a decrease in upstream flow depth. Also, it should be noted that the fluid flow, at leading order, encounters the slow moving step in bedforms as if it were stationary. This is borne out in (39*a*) which simply expresses conservation of fluid mass for steady flow over a fixed step.

Finally, we calculate the Froude numbers relative to the discontinuity both ahead and behind as

$$F_R = F_o, \quad F_L = F_o/H^{\frac{3}{2}}, \tag{39c}$$

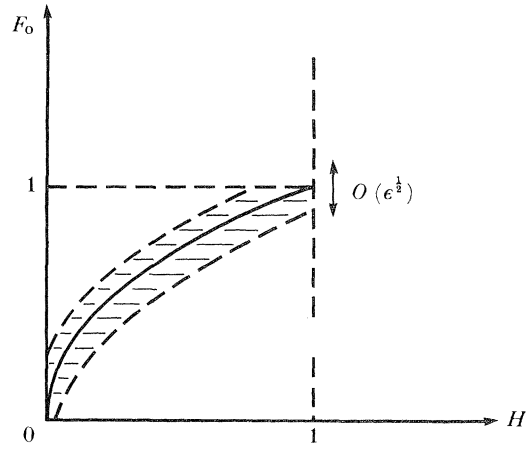

Figure 7. The region of non-uniformity of the $\dot{s}_-$, $\dot{s}_b$ waves in the (H, F_o) plane.

respectively. Since this family of solutions requires $H < 1$, we observe that,

$$F_L > F_R. \tag{40}$$

The domain of existence of the family of solutions is shown in figure 6*a*, while illustrations of typical solutions from this family are shown in figure 6*b*, *c*.

This family of solutions, which has no analogue in fixed-bed hydraulics, exhibits the required properties to describe the observed, slow moving, sediment bores. However, further discussion and comparison is postponed until the remaining details of the full set of solutions have been completed.

9. Non-uniform behaviour in the approximations for $\epsilon \ll 1$

In the previous section we have developed a theory for simple wave solutions through solving the cubic equation (25) for $\epsilon \ll 1$ with $H, F_o > 0$. The solution has two roots of $O(1)$, $\dot{s}_\pm$, and a single root of $O(\epsilon)$, $\dot{s}_b$. As in the case of the linearized theory (Needham 1990) the approximations associated with the $\dot{s}_-$ and $\dot{s}_b$ roots become non-uniform over a localized region of the (H, F_o) plane. This is evident from the singular behaviour in the leading-order approximation for $\dot{s}_b$, (34), along the curve $G(H, F_o) = 0$ in $H < 1$. The non-uniformity in $\dot{s}_-$ also occurs along $G(H, F_o) = 0$ in $H < 1$, and is reflected through the singular behaviour in the associated $\tilde{\xi}_L$, (31*b*). The approximation to the root $\dot{s}_+$ remains regular throughout the whole of its domain of definition, $H > 1$.

We now examine the behaviour of $\dot{s}_b$ and $\dot{s}_-$ in the neighbourhood of $G(H, F_o) = 0$; that is, when $F_o \sim \sqrt{(\frac{1}{2}H(H+1))}$ with $0 < H < 1$. A consideration of equation (25) reveals that the region of non-uniform behaviour is $F_o = \sqrt{(\frac{1}{2}H(H+1))} + O(\epsilon^{\frac{1}{2}})$ with $0 < H < 1$ as $\epsilon \to 0$, which is in accord with the linearized theory of Needham (1990). A sketch of the region of non-uniform behaviour is shown on the (H, F_o) plane in figure 7. Within this region, (26) and (34) indicate that $\dot{s}$ is of $O(\epsilon^{\frac{1}{2}})$. To formalize the region we introduce the variable $\tilde{F}_o$, where,

$$F_o = \sqrt{(\tfrac{1}{2}H(H+1))} + \epsilon^{\frac{1}{2}}\tilde{F}_o; \quad 0 < H < 1, \tag{41}$$

with $\tilde{F}_o$ of $O(1)$, and write,

$$\dot{s} = \epsilon^{\frac{1}{2}} U, \tag{42}$$

with U of $O(1)$.

We use (41) and (42) to replace $\dot{s}$ and F_o in equation (25). At leading order (25) reduces to a quadratic equation in U, the two roots of which lead to the wave speeds,

$$\dot{s} = \dot{S}_{\pm} \sim \epsilon^{\frac{1}{2}} \left\{ \frac{2^{\frac{1}{2}} \tilde{F}_o}{\sqrt{(\frac{1}{2}H(H+1))}} \pm \frac{1}{2} \sqrt{\left(\frac{2\tilde{F}_o^2}{H(H+1)} + \frac{2(H+1)}{H} \right)} \right\}, \tag{43}$$

as $\epsilon \to 0$ in the region defined by (41). We note that $\dot{S}_{\pm}$ are real throughout this region, with

$$\dot{S}_+ > 0, \quad \dot{S}_- < 0 \quad \forall\, 0 < H < 1, \quad |\tilde{F}_o| < \infty. \tag{44}$$

Moreover, as we move out of region (41), with H fixed, we observe from (43), that

$$\dot{S}_+ \to \begin{cases} \dot{s}_-; & \tilde{F}_o \to +\infty, \\ \dot{s}_b; & \tilde{F}_o \to -\infty, \end{cases}$$

$$\dot{S}_- \to \begin{cases} \dot{s}_b; & \tilde{F}_o \to +\infty, \\ \dot{s}_-; & \tilde{F}_o \to -\infty. \end{cases} \tag{45}$$

Thus $\dot{S}_+$ continues $\dot{s}_b$ in $F_o < \sqrt{(\frac{1}{2}H(H+1))}$ into $\dot{s}_-$ in $F_o > \sqrt{(\frac{1}{2}H(H+1))}$, whilst $\dot{S}_-$ continues $\dot{s}_-$ in $F_o < \sqrt{(\frac{1}{2}H(H+1))}$ into $\dot{s}_b$ in $F_o > \sqrt{(\frac{1}{2}H(H+1))}$.

To complete the details we obtain the jumps in $\bar{\xi}$ and v associated with $\dot{S}_{\pm}$ from (24a, b) as

$$[v^{\pm}]_R^L = [\hat{v}^{\pm}]_R^L \sim \frac{1}{H} - 1 > 0, \tag{46a}$$

$$[\bar{\xi}^{\pm}]_R^L = \bar{\xi}_L \sim \epsilon^{\frac{1}{2}} (1-H^2)/H^2 \left\{ \frac{2^{\frac{1}{2}} \tilde{F}_o}{2\sqrt{(H(H+1))}} \pm \frac{1}{2} \sqrt{\left(\frac{2\tilde{F}_o^2}{H(H+1)} + \frac{2(H+1)}{H} \right)} \right\} \quad \begin{cases} > 0; \dot{S}_+, \\ < 0; \dot{S}_-. \end{cases} \tag{46b}$$

An examination of (43) and (46a, b) shows that both of the $\dot{S}_{\pm}$ waves are slow moving, with speeds of $O(\epsilon^{\frac{1}{2}})$ and carry with them an $O(\epsilon^{\frac{1}{2}})$ step in bedform. The $\dot{S}_+$ wave moves downstream with a step-down in bedform and the step in flow depth is in antiphase to the bedform step. The $\dot{S}_-$ wave propagates upstream, carrying a step-up in bedform, with the step in flow depth now in phase with the bedform step.

The continuation properties (45) of the $\dot{S}_{\pm}$ families of solutions in region (41) can now be used to develop a more concise notation for the complete family of solutions which exist in the region $0 < H < 1$ of the (H, F_o) plane.

10. A concise notation

The continuation properties (45) of the $\dot{S}_{\pm}$ families of solutions in region (41) enable a more concise notation to be developed to describe the families of solutions obtained throughout the (H, F_o) plane. The complete set of families of solutions obtained in the previous sections can be grouped into three families which we shall denote by C_1, C_2 and C_3 waves, which are defined below.

10.1. C_3 *waves*

This family of solutions includes those in $H > 1$ with speed $\dot{s}_+$. Thus C_3 waves are defined in $H > 1$ and have positive wave speeds

$$c_3 \sim \dot{s}_+; \quad H > 1. \tag{47}$$

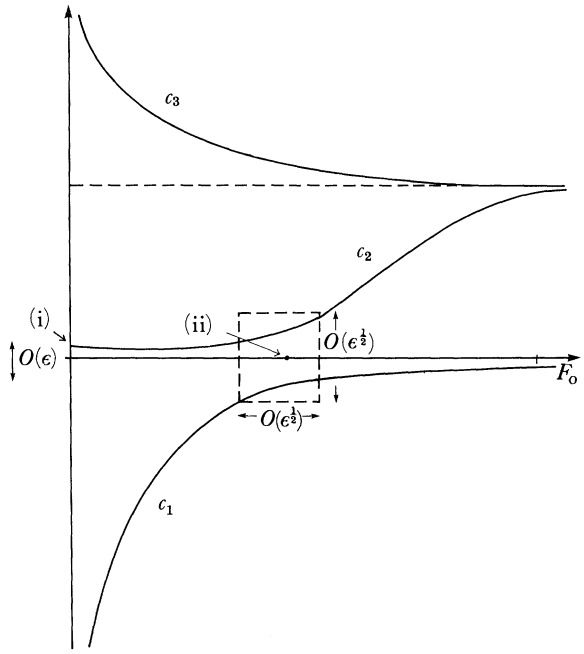

Figure 8. The wave speeds c_1, c_2, c_3 as functions of F_0 with $H < 1$ fixed; (i) $\epsilon(H+1)/H^2$, (ii) $\sqrt{\frac{1}{2}}(H(H+1))$.

The jumps in h, v, $\bar{\xi}$ for this family of solutions are then,

$$[h]^{\mathrm{L}}_{\mathrm{R}} = (H-1) > 0, \tag{48a}$$

$$[v]^{\mathrm{L}}_{\mathrm{R}} = [\hat{v}]^{\mathrm{L}}_{\mathrm{R}} = [v_+]^{\mathrm{L}}_{\mathrm{R}} > 0, \tag{48b}$$

$$[\bar{\xi}]^{\mathrm{L}}_{\mathrm{R}} = [\bar{\xi}_+]^{\mathrm{L}}_{\mathrm{R}} > 0. \tag{48c}$$

For a given $H > 1$, the wave speed c_3 is a monotone decreasing function of F_0, and a sketch is given in figure 8 on the (c_3, F_0) plane.

10.2. C_2 *waves*

This family of solutions is defined throughout the region $0 < H < 1$ and represents the composite of the $\dot{s}_-$, $\dot{S}_+$ and $\dot{s}_b$ families. Its wave speed c_2 is continuous and positive throughout the whole of $0 < H < 1$ and is given by (from (26), (34), (41), (43), (45)),

$$c_2 \sim \begin{cases} \dot{s}_b; & 0 < F_0 < \chi(H) - O(\epsilon^{\frac{1}{2}}) \\ \dot{S}_+; & \chi(H) - O(\epsilon^{\frac{1}{2}}) < F_0 < \chi(H) + O(\epsilon^{\frac{1}{2}}) \\ \dot{s}_-; & F_0 > \chi(H) + O(\epsilon^{\frac{1}{2}}) \end{cases}, \tag{49}$$

where $\chi(H) = \sqrt{(\frac{1}{2}H(H+1))}$ and $\tilde{F}_0$ is defined in (41). With a given $H < 1$, a sketch of the wave speed c_2 in the (c_2, F_0) plane is shown in figure 8. The associated jumps from the C_2 wave are given by

$$[h]^{\mathrm{L}}_{\mathrm{R}} = (H-1) < 0, \tag{50a}$$

$$[v]^{\mathrm{L}}_{\mathrm{R}} = [\hat{v}]^{\mathrm{L}}_{\mathrm{R}} \sim \begin{cases} [v_{\mathrm{b}}]^{\mathrm{L}}_{\mathrm{R}} > 0; & 0 < F_0 < \chi(H) + O(\epsilon^{\frac{1}{2}}), \\ [v_-]^{\mathrm{L}}_{\mathrm{R}} > 0; & F_0 > \chi(H) + O(\epsilon^{\frac{1}{2}}), \end{cases} \tag{50b}$$

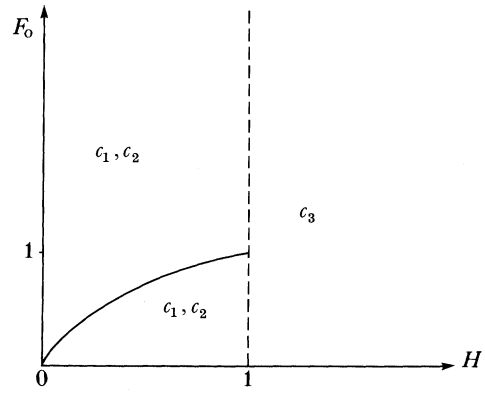

Figure 9. The domains of existence of the c_1, c_2, c_3 waves in the (H, F_o) plane, with the transitional behaviour in c_1 and c_2 occurring across $F_o = \frac{1}{2}\sqrt{(H(H+1))}$.

$$[\bar{\xi}]^{\mathrm{L}}_{\mathrm{R}} \sim \begin{cases} [\bar{\xi}_{\mathrm{b}}]^{\mathrm{L}}_{\mathrm{R}} > 0; & 0 < F_o < \chi(H) - O(\epsilon^{\frac{1}{2}}), \\ [\bar{\xi}^{+}]^{\mathrm{L}}_{\mathrm{R}} > 0; & \chi(H) - O(\epsilon^{\frac{1}{2}}) < F_o < \chi(H) + O(\epsilon^{\frac{1}{2}}), \\ [\bar{\xi}_{-}]^{\mathrm{L}}_{\mathrm{R}} > 0; & F_o > \chi(H) + O(\epsilon^{\frac{1}{2}}). \end{cases} \tag{50c}$$

Thus the C_2 wave has speed $c_2 > 0$ throughout $0 < H < 1$, with $\bar{\xi}_{\mathrm{L}} > 0$ and the step in bedform is in antiphase with the step in flow depth.

10.3. C_1 *waves*

This family of solutions is defined throughout the region $0 < H < 1$ and represents the composite of the $\dot{s}_-$, $\dot{S}_-$ and $\dot{s}_{\mathrm{b}}$ families. The wave speed c_1 is continuous and negative throughout the region $0 < H < 1$ and is given by (from (26), (34), (43), (45)),

$$c_1 \sim \begin{cases} \dot{s}_-; & 0 < F_o < \chi(H) - O(\epsilon^{\frac{1}{2}}), \\ \dot{S}_-; & \chi(H) - O(\epsilon^{\frac{1}{2}}) < F_o < \chi(H) + O(\epsilon^{\frac{1}{2}}), \\ \dot{s}_{\mathrm{b}}; & F_o > \chi(H) + O(\epsilon^{\frac{1}{2}}). \end{cases} \tag{51}$$

For a given $H < 1$, a sketch of c_1 as a function of F_o is shown in figure 8. The corresponding jumps for the C_1 wave are given by,

$$[h]^{\mathrm{L}}_{\mathrm{R}} = (H-1) < 0, \tag{52a}$$

$$[v]^{\mathrm{L}}_{\mathrm{R}} = [\acute{v}]^{\mathrm{L}}_{\mathrm{R}} \sim \begin{cases} [v_-]^{\mathrm{L}}_{\mathrm{R}} > 0; & 0 < F_o < \chi H) - O(\epsilon^{\frac{1}{2}}), \\ [v_{\mathrm{b}}]^{\mathrm{L}}_{\mathrm{R}} > 0; & \chi(H) - O(\epsilon^{\frac{1}{2}}) < F_o < \sqrt{(\tfrac{1}{2}(H/H-1))} \end{cases} \tag{52b}$$

$$[\bar{\xi}]^{\mathrm{L}}_{\mathrm{R}} = \bar{\xi}_{\mathrm{L}} \sim \begin{cases} [\bar{\xi}_-]^{\mathrm{L}}_{\mathrm{R}} < 0; & 0 < F_o < \chi(H) - O(\epsilon^{\frac{1}{2}}), \\ [\bar{\xi}^-]^{\mathrm{L}}_{\mathrm{R}} < 0; & \chi(H) - O(\epsilon^{\frac{1}{2}}) < F_o < \chi(H) + O(\epsilon^{\frac{1}{2}}), \\ [\bar{\xi}_{\mathrm{b}}]^{\mathrm{L}}_{\mathrm{R}} < 0; & F_o > \chi(H) + O(\epsilon^{\frac{1}{2}}). \end{cases} \tag{52c}$$

Hence, the C_1 wave has speed $c_1 < 0$ throughout its domain of definition $0 < H < 1$, with $\bar{\xi}_{\mathrm{L}} < 0$, and the step in bedform in phase with the step in flow depth.

In the limit as $H \to 1$, the three families of solutions $C_i\,(i = 1, 2, 3)$ reduce to those described in the linearized theory of Needham (1990). A sketch of the domains of definition of the $C_i\,(i = 1, 2, 3)$ families of solutions is shown in figure 9.

We next consider the generation of $C_i\,(i = 1, 2, 3)$ simple waves by a prescribed upstream change in the sediment discharge rate.

11. The generation of simple waves

Here we consider the possibility of a specified change in the upstream sediment discharge rate leading to the development of propagating, discontinuous, simple waves of the type belonging to the families $C_i\,(i = 1, 2, 3)$. Since the change in sediment discharge rate is specified upstream, any waves which subsequently develop must propagate downstream (out going waves). Thus the only type of discontinuous simple waves which may be generated are (via (47), (49), (51)) those in the C_2 and C_3 families. Moreover, we note from (48*b*) and (50*b*) that simple waves in both of these families have $[v]^{\mathrm{L}}_{\mathrm{R}} > 0$, which, through (13*d*), leads to $[q]^{\mathrm{L}}_{\mathrm{R}} > 0$. This condition implies that discontinuous simple waves of the type C_2 and C_3 can only develop following an upstream increase in the sediment discharge rate. It is expected that a decrease in the upstream sediment discharge rate will not lead to a steepening bedform, but a bedform which will propagate with a shallow gradient in the form of a continuous expansion wave.

In this paper we are concerned with the formation and propagation of sediment bores. As noted in the introduction, the formation of a sediment bore generally follows an increase in the upstream sediment discharge rate, which is in line with the above discussion on the development and propagation of C_2 and C_3 waves. The characteristic features of the sediment bore are its slow speed of propagation (relative to the flow speed) and its significant step in bedform (comparable in height with the local flow depth). These properties are not apparent in the C_3 wave, which propagates with a speed (47), which is comparable with the flow speed, and carries only a small step in bedform, with a height, (48*c*), much less than that of the local flow depth. However, from (49) and (50*c*), we see that the C_2 wave has a slow speed of propagation and carries an $O(1)$ step in bedform in the region,

$$0 < F_0 < \chi(H) - O(\epsilon)^{\frac{1}{2}}, \quad 0 < H < 1, \tag{53}$$

but suffers a transition across the boundary $F_0 = \chi(H)$. Thus the C_2 wave, restricted to region (53), exhibits the major features of a sediment bore. We therefore identify the C_2 wave in region (53) with a sediment bore and limit further attention to this case.

It is worth noting at this stage that the differential forms of the integral conservation laws (13*a–d*) represent a third order hyperbolic system, and the particular solutions considered in the present paper represent simple waves generated by discontinuities forming on each of the three distinct characteristic families associated with the system. Moreover, following the linearized theory of Needham (1990), the system can be shown to be of wave hierarchy type, with three dynamic waves (from which the C_1, C_2, C_3 waves of the present paper are special discontinuous solutions), and two kinematic waves. One kinematic wave has an $O(1)$ speed and carries only an $O(\epsilon)$ step in bedform, limiting to the usual flood wave of fixed bed hydraulics as $\epsilon \to 0$. The other does not propagate and is purely diffusive, corresponding to erosion of stationary bedforms. Neither of the two kinematic waves can be associated with propagating bedforms.

As seen in the present paper, propagating bedforms are associated with the C_2, C_1 type dynamic waves. A further interesting interpretation can be made when conditions are such that $F_0 \sim \sqrt{(\frac{1}{2}H(H+1))}$, $H < 1$, and the C_1, C_2 waves are in transition from bedform to river waves and vice versa, as discussed in §9. Under these conditions the interaction between surface and bedform wave is strongest, with

C_1, C_2 being fully coupled surface and bedform waves. In addition, using (41) and (46), we have $F_L > 1$ and $F_R < 1$ for both of these waves in this region. This stronger interaction between the bedform and surface wave, and the subcritical–supercritical transition over the wave front are characteristic of anti-dune propagation and we tentatively speculate that this interaction when $F_o \sim \sqrt{(\frac{1}{2}H(H+1))}$ in $H < 1$ may be related to anti-dune formation.

12. Discussion of the sediment bore solutions

We have identified sediment bores with the C_2 family of discontinuous simple waves, when restricted to the domain in the (H, F_o) plane described by (53). A further physical requirement for the observation of a sediment bore in this region of the (H, F_o) parameter space is that the sediment bore be temporally stable. A criterion for stability may be obtained from the linearized theory of Needham (1990). In that paper, with $\epsilon \ll 1$, it is shown that the leading order stability requirement for a uniform alluvial flow with Froude number, F, is

$$F < 2. \tag{54}$$

The simple wave solution representing a sediment bore is constructed from two uniform alluvial flows with differing Froude numbers F_L and F_R, upstream and downstream of the discontinuity respectively. Therefore, on using condition (54), we deduce that a sediment bore solution will be temporally stable provided

$$\max\{F_L, F_R\} < 2. \tag{55}$$

After use of (39c) condition (55) reduces to

$$F_o < 2H^{\frac{3}{2}}. \tag{56}$$

This stability requirement restricts further the domain (53). Stable sediment bore solutions now exist only in the domain,

$$\left.\begin{aligned} 0 < F_o < 2H^{\frac{3}{2}}, &\quad 0 < H \leqslant 0.42153, \\ 0 < F_o < \chi(H), &\quad 0.42153 < H < 1, \end{aligned}\right\} \tag{57}$$

where $H = 0.42153$ is the point of intersection of the functions $\chi(H)$ and $2H^{\frac{3}{2}}$.

In deriving the family of sediment bore solutions, we have used H and F_o as parameters. In practice, it is the upstream sediment discharge rate, q_L, which is specified, rather than the flow depth, H. On examining the features of the family of sediment bore solutions it is therefore more appropriate to work in the (q_L, F_o) plane. The parameters H and q_L are related, via (13d) and (39a), by

$$q_L = 1/H^2. \tag{58}$$

On using (58) to transform (57) into the (q_L, F_o) plane, we obtain,

$$\left.\begin{aligned} 1 < q_L < (4/F_o^2)^{\frac{2}{3}}, &\quad 0 < F_o < 0.54736, \\ 1 < q_L < 4/(\sqrt{(1+8F_o^2)}-1)^2, &\quad 0.54736 < F_o < 1, \end{aligned}\right\} \tag{59}$$

as the domain in which stable sediment bore solutions exist. A sketch of this domain on the (q_L, F_o) plane is shown in figure 10. An examination of figure 10 shows that sediment bores will only develop for $q_L > 1$, that is an increase in the upstream sediment discharge rate, and also require the uniform flow ahead to be subcritical, i.e. $F_o < 1$. Moreover, for each $F_o < 1$, there is a cut-off value for q_L above which sediment bores will not occur. This cut-off value increases unboundedly as $F_o \to 0$, but

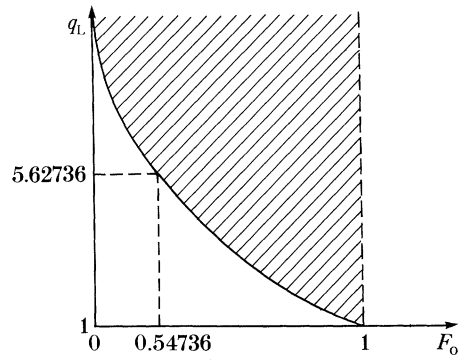

Figure 10. The domain of existence of sediment bores in the (F_o, q_L) plane.

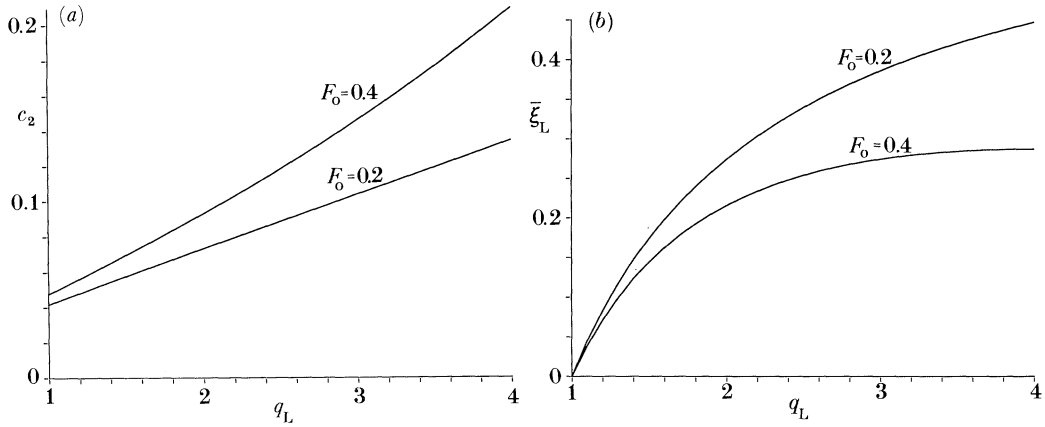

Figure 11. The sediment bore characteristics when $F_o = 0.2, 0.4$ with $\epsilon = 0.02$ and $1 \leqslant q_L \leqslant 4$ (*a*) c_2 against q_L, (*b*) $\bar{\xi}_L$ against q_L.

decreases to unity as $F_o \to 1$. The cut-off values of q_L are provided by the upper limits in (59). In terms of q_L and F_o, the properties of the family of sediment bore solutions become, from (49) and (50),

$$c_2 \sim \epsilon(1+q_L^{\frac{1}{2}})^2/q_L^{\frac{1}{2}} g(q_L, F_o), \quad H \sim 1/q_L^{\frac{1}{2}}, \quad v_L \sim q_L^{\frac{1}{2}}, \tag{60a–c}$$

$$\bar{\xi}_L \sim q_L^{\frac{1}{2}}(q_L^{\frac{1}{2}}-1)\, g(q_L, F_o)/(q_L^{\frac{1}{2}}+1), \tag{60d}$$

where $g(q_L, F_o) = q_L^{-1}\{1+q_L^{\frac{1}{2}}\} - 2F_o^2$.

An examination of (60*a–d*) reveals the qualitative behaviour of the properties associated with the sediment bore as q_L is varied for fixed F_o. With q_L close to its lower limit of unity, $\bar{\xi}_L \to 0$ and $c_2 \to 2\epsilon/(1-F_o^2)$, the linearized wave speed given in Needham (1990). As q_L increases, $\bar{\xi}_L$ achieves a local maximum, after which it decreases, before finally becoming small, of $O(\epsilon^{\frac{1}{2}})$, as q_L approaches its upper cut-off limit. The behaviour of c_2 is monotone increasing with q_L, becoming of $O(\epsilon^{\frac{1}{2}})$ as the upper limit for q_L is reached.

To obtain a quantitative picture, we consider two cases in detail. In both cases $\epsilon = 0.02$, whilst case one has $F_o = 0.2$ and case two has $F_o = 0.4$. Sediment bores exist for $1 < q_L < q_L^*$ where $q_L^* = 21.5443$ and 8.5499 in cases one and two respectively. However, in most practical situations, the upstream increases in sediment discharge

will not exceed a four-fold increase, and in both cases we restrict $1 < q_L < 4$. In figure 11*a* the sediment bore propagation speed, c_2, is plotted against $1 < q_L < 4$ for both cases. These show that c_2 increases with q_L, whilst there is an overall increase in c_2 from the case $F_0 = 0.2$ to the case $F_0 = 0.4$ in line with (60*a*) which is a montone increasing function of F_0 at fixed q_L. In figure 11*b* the step in bedform, $\bar{\xi}_L$, is plotted against $1 < q_L < 4$ for both cases. In the case of $F_0 = 0.2$, $\bar{\xi}_L$ is a monotone increasing function on $0 < q_L < 4$, with its maximum achieved at a value of $q_L > 4$. However, for the case $F_0 = 0.4$, the maximum value of $\bar{\xi}_L$ is approached at the end of the range $0 < q_L < 4$, and we observe the beginning of the decrease in $\bar{\xi}_L$, which must become of $O(\epsilon^{\frac{1}{3}})$ as $q_L \to q_L^*$ and the transition region is approached. We also note the overall decrease in $\bar{\xi}_L$ from the case $F = 0.2$ to $F = 0.4$. This can be deduced from (60*d*), which is a montone decreasing function of F_0 at fixed q_L.

13. The generation of a sediment bore in the flume

As mentioned in the introduction, the generation of a sediment bore in a flume is quite straightforward, requiring the maintainence of a one- or two-fold increase in the sediment supply of an otherwise uniform alluvial flow. We have done a simple experiment of this type in the flume at UEA, which is described below. Measurements were made throughout the experiment and are compared with theoretical predictions at the end of this section.

At the beginning of the experiment the dry flume was prepared with a 3 cm level bed of 2 mm grit. A uniform alluvial flow was then generated by introducing a water discharge per unit width at the head of the flume of 0.036 $m^2\ s^{-1}$. This discharge rate was calculated using the flow meter on the return pipe of the flume. At equilibrium the uniform flow was found to carry a volumetric bed-load sediment transport rate per unit width of $3.666 \times 10^{-6}\ m^2\ s^{-1}$ (all the sediment was transported as bedload). This was measured by collecting sediment discharged at the end of the flume. This transport rate was maintained by supplying sediment uniformly across the flume at the required rate, by means of a hopper situated at the head of the flume.

To make measurements, two of the flume side windows (the first situated about 1.5 m downstream from the head of the flume) were marked with a coordinate grid of dimensions 10 cm × 3 cm. A photograph of the uniform flow through the first of these windows is shown in figure 12.

To generate the sediment bore, a sudden and sustained increase was made to the sediment supply from the hopper at the head of the flume, at reference time, $t =$ 0 min. The immediate response to this was a large buildup of sediment at the head of the flume with a corresponding rapid contraction in flow depth in the vicinity of the sediment buildup. Over the first 10 min the flow began to erode this local buildup of sediment by initiating the formation of a sediment bore. In its transient stages, the step height of the sediment bore and its speed of propagation varied quite considerably. Also, small disturbances which appeared behind the bore where observed to rapidly catch up with it, whilst small disturbances ahead were caught up by the bore. This observation is in line with the theory, in which the sediment bore is obtained as a discontinuous simple wave solution of the system of conservation laws (1)–(4) which, in differential form are of hyperbolic type. Thus the characteristic slope associated with the state behind the discontinuity must be larger than that corresponding to the state ahead of the discontinuity. Small disturbances both ahead

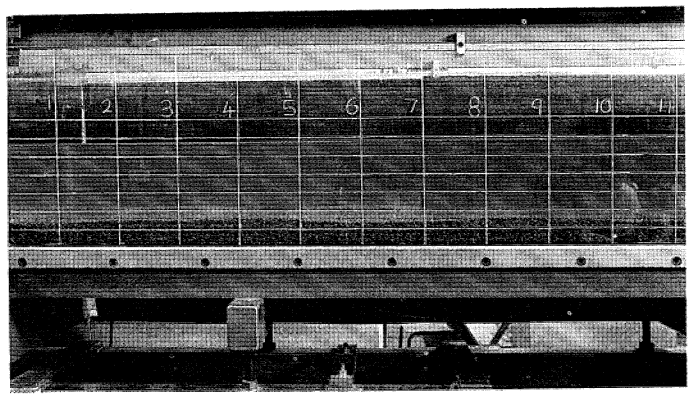

Figure 12. The uniform alluvial flow viewed through window 1.

and behind propagate along these characteristic slopes and are therefore enveloped by the discontinuity, in line with the above observation. Photographs of the developing sediment bore where taken at times $t = 11$, 13, 15, 17 min during this transient stage, when the wave front was propagating through the first of the two observation windows. These are shown in figure 13*a–d*. The mean propagation speed of the sediment bore at this stage is estimated at approximately 1.5×10^{-3} m s^{-1}. A further feature to note is the small disturbance which forms behind the wave front in the photograph at time $t = 15$ min. At the later time $t = 17$ min this has developed and is rapidly advancing upon the primary bore wave front, as predicted by the theory. The propagation speed of this wavelet is estimated at 2.9×10^{-3} m s^{-1}.

After a further 13 min, at $t = 30$ min, the sediment bore had reached its quasi-steady equilibrium form, maintaining a constant step height in bedform and propagating with a constant speed. At this stage the bore wave front had reached the second observation window. Photographs are shown in figure 14*a–d* at times $t = 30$, 40, 50, 60 min. The bore has reached its constant equilibrium propagation speed which is estimated from figure 14*a–d* as 1.67×10^{-4} m s^{-1}. A point worth comment is that the wave front in figure 14*a–d* does not appear as a discontinuity, but has a linear slope over a horizontal length scale comparable to the mean flow depth. This is not in conflict with the theory, since the shallow water theory is based on a horizontal length scale derived from the mean flow depth and the very small overall slope of the river flow. When measured relative to this shallow water length scale, the slope at the wave front is very large, approaching a discontinuity in the shallow water limit adopted in the theory.

The photographs in figure 14*a–d* enable us to determine the depth both upstream and downstream of the sediment bore as 0.09 m and 0.15 m respectively. Since the wave front of the bore is moving extremely slowly relative to the water flow speed, we are then able to use the known water discharge of 0.036 m^2 s^{-1} to estimate the depth averaged water velocity as 0.4 m s^{-1} and 0.24 m s^{-1} upstream and downstream of the wave front respectively. With these measurements we obtain the upstream and downstream Froude numbers as 0.426 and 0.198 respectively. To determine the increased rate of sediment transport behind the step we first calculate the volume of sediment stored in the bed-step by the advancing wave front from the photographs at $t = 30$ and $t = 50$ min, from which we subtract the volume of sediment transported away from the step at the known downstream transport rate, over the same time

PHILOSOPHICAL TRANSACTIONS OF THE ROYAL SOCIETY A MATHEMATICAL, PHYSICAL & ENGINEERING SCIENCES

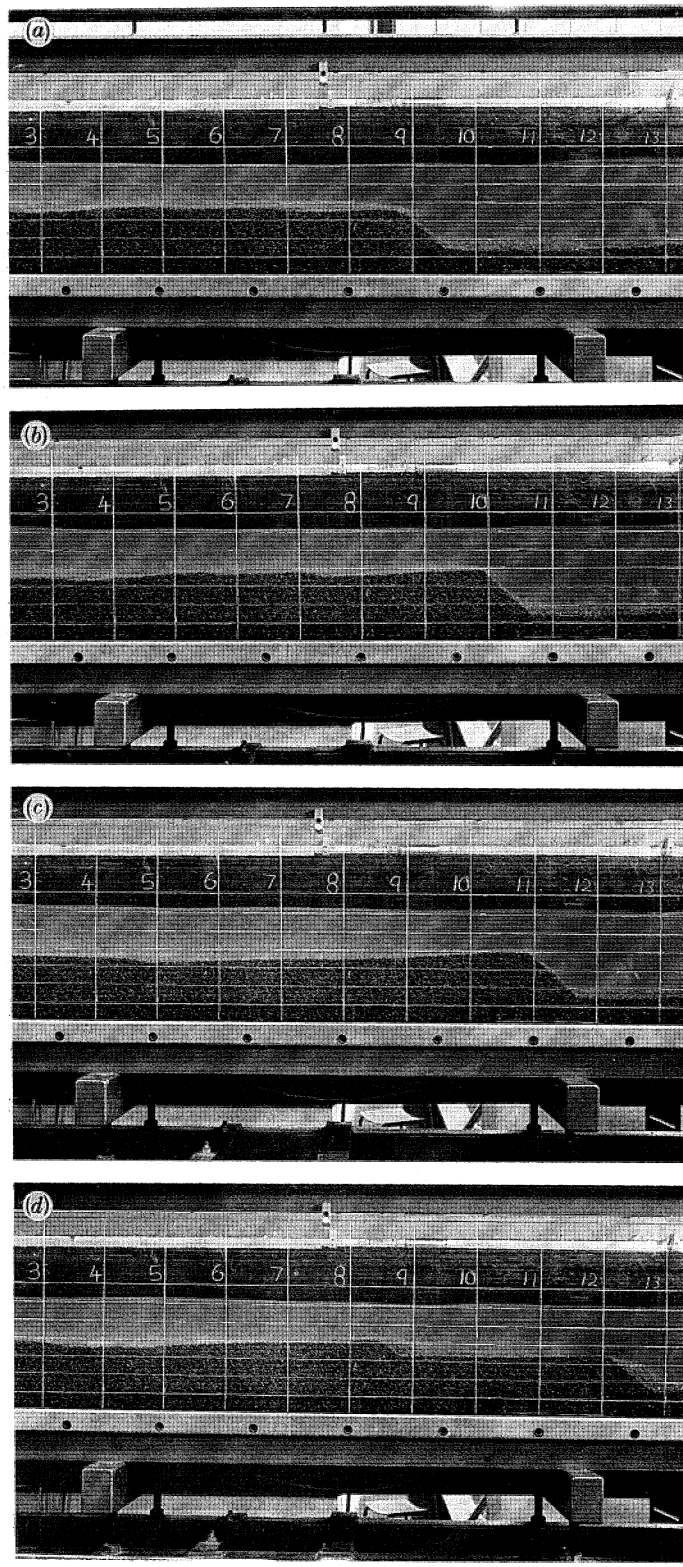

Figure 13. The transient stage in the formation of the sediment bore viewed through window 1 at times $t =$ (*a*) 11 min, (*b*) 13 min, (*c*) 15 min, (*d*) 17 min.

PHILOSOPHICAL TRANSACTIONS OF THE ROYAL SOCIETY A MATHEMATICAL, PHYSICAL & ENGINEERING SCIENCES

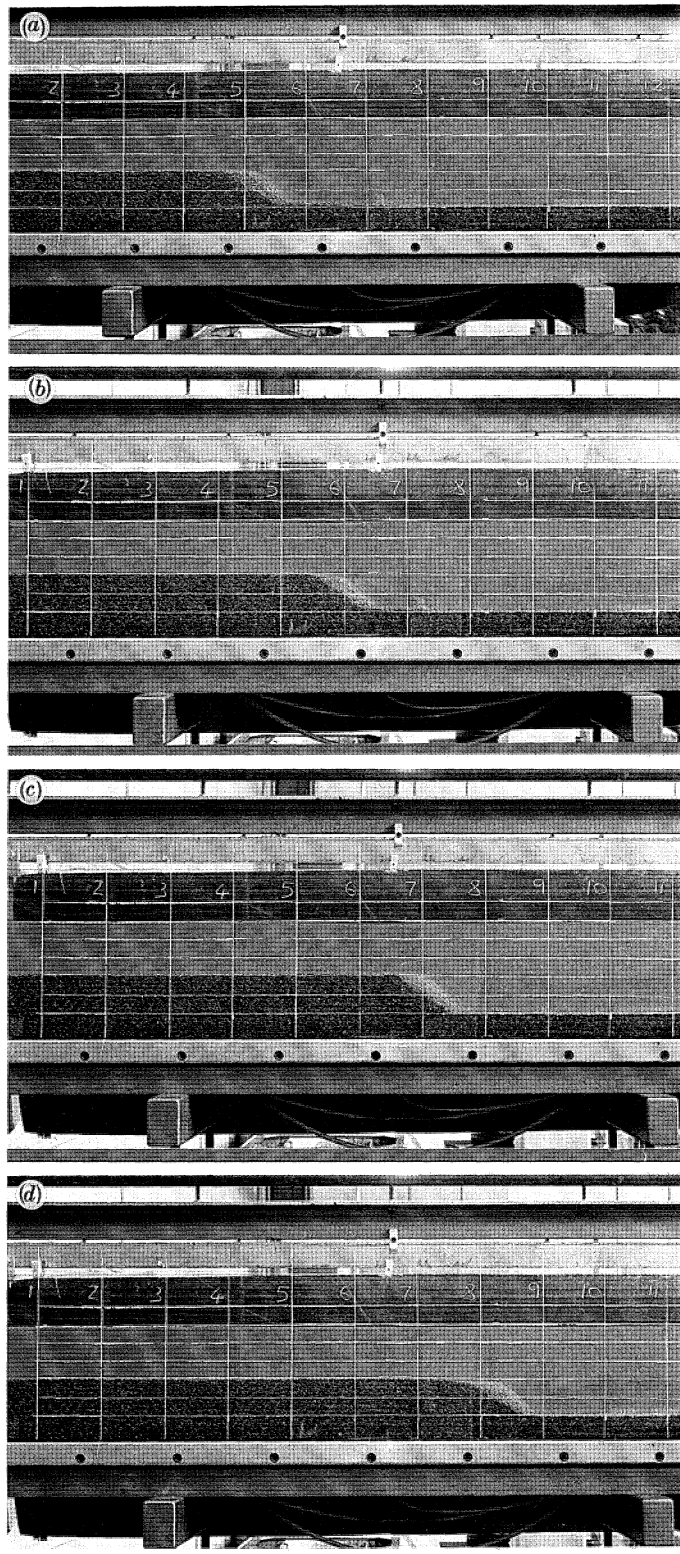

Figure 14. The quasi-steady sediment bore viewed through window 2 at times $t =$ (*a*) 30 min, (*b*) 40 min, (*c*) 50 min, (*d*) 60 min. The photographs were produced in the flume at UEA.

PHILOSOPHICAL TRANSACTIONS OF THE ROYAL SOCIETY A MATHEMATICAL, PHYSICAL & ENGINEERING SCIENCES

interval. This leads to a value of $1.0 \times 10^{-5}\ \mathrm{m^2\ s^{-1}}$ for the increased upstream sediment discharge rate per unit width.

We can now compute the parameters ϵ, F_o, q_L required by the theory. From above, the downstream Froude number is $F_o = 0.198$. The parameter q_L is the ratio of the upstream to downstream bed-load sediment transport rates, thus we have $q_L = 2.78$. Finally ϵ is the ratio of the downstream sediment discharge rate to the water discharge rate, which gives $\epsilon = 10^{-4}$. These parameter values are used to obtain the theoretical predictions for the bedform step height and the propagation speed of the sediment bore. After substitution into equations (60*a*, *d*) we obtain,

$$\bar{\xi}_{\mathrm{th}} = 0.368, \quad c_{2,\mathrm{th}} = 4.84 \times 10^{-4} \tag{61}$$

as theoretical predictions (to three significant figures). The experimental values for these quantities are obtained, via the photographs in figures 14*a–d*, as

$$\bar{\xi}_{\mathrm{exp}} = 0.4, \quad c_{2,\mathrm{exp}} = 5.56 \times 10^{-4}. \tag{62}$$

A comparison of (61) and (62) shows at least an order of magnitude agreement in both quantities. In fact the percentage error in the bedstep height is 8%, while that in the bore propagation speed is 12.9%. This level of agreement is very encouraging, particularly since it has been obtained through a relatively unsophisticated level of experimentation. A point worth noting is that the only empiricism in the theory is introduced through the sediment transport function, which is taken to have the form $q = mv^2$; thus we would expect the quantitative accuracy of the theory to depend upon the applicability of this transport function. We can examine how accurate this transport function is for the present case by using the above data. On using the measured values of q and v ahead of the wave we obtain an estimate for m as $m = 6.37 \times 10^{-5}$ s. With this value for m, the sediment transport rate behind the wave would then be predicted as $1.019 \times 10^{-5}\ \mathrm{m^2\ s^{-1}}$, whereas the measured value was recorded as $1.0 \times 10^{-5}\ \mathrm{m^2\ s^{-1}}$. Therefore the sediment transport function used in the theory is in error by 1.87% in predicting the upstream transport rate, when calibrated on the downstream conditions. This remarkable level of accuracy of the quadratic sediment transport function is in line with the levels of agreement between (61) and (62).

Finally, we comment on the form of the free surface of the water. From the photographs in figure 14*a–d* we see that the deflection in the free surface of the water as it flows over the step in bedform is negligible, of the order of 5 mm at the end of the observation window. The theory predicts a change in the free surface level, via (60*d*, *b*), as 4.8 mm. This is in agreement with the above observation up to 4%. Also, since the flow downstream of the step in bedform is subcritical, it is interesting to consider why steady gravity waves are not observed on the surface of the water in figure 14*a–d* downstream of the step. To address this point, we first note that since the propagation speed of the step in bedform is slow compared with the mean flow velocity of the water; as a first approximation we may consider the step as being stationary. We can then draw some conclusions using the theory of King & Bloor (1987) who address the problem of steady free surface flow over a rigid, fixed step in the bed. This theory predicts the presence of a downstream gravity wave train, when the flow is subcritical. However, for the parameters in the present experiment, the wave length of these gravity waves is predicted as *ca.* 567 cm, with an amplitude of *ca.* 4.6 cm. This leads to a free surface slope of *ca.* 8×10^{-3}. Thus the waves are not

PHILOSOPHICAL TRANSACTIONS OF THE ROYAL SOCIETY A MATHEMATICAL, PHYSICAL & ENGINEERING SCIENCES

detectable over the length of the observation window which is in line with the photographs in figure 14*a–d*.

A further point to note is the structure of the sediment bore wave front as shown in figure 14*a–d*. As discussed above, the change in free surface level over the wave front is negligible while the change in bedform level over the wave front is linear. This is in line with our proposed form for the function $d'(y)$ in (18*a*).

The experiment which has been described in this section has readily reproduced the qualitative features predicted by the theory. However, it has also shown that the quantitative predictions of the theory are in line with observations, which is encouraging for the theory.

14. Conclusions

We have considered the integral conservation laws governing one-dimensional hydraulic flows in alluvial rivers or channels. In particular we have examined those simple wave solutions which have a step discontinuity in bedform and free surface, separating two differing, upstream and downstream, uniform alluvial flows. This type of solution may be generated by a change in the order of magnitude of the upstream sediment discharge rate, q_L, in an otherwise uniform alluvial flow. We have shown that there are three families of solutions of this type, each family parametrized by the upstream sediment discharge rate q_L and the downstream Froude number, F_0. In a restricted region of the (F_0, q_L) plane, one of these families of solutions has the appropriate form to represent a stable sediment bore. The detailed properties of this family of solutions have been obtained, for example the step in bedform height, the propagation speed, and the step in free surface level, as functions of q_L and F_0.

In particular it has been shown that the downstream propagation of a stable sediment bore requires:

(1) an increase in the upstream rate of sediment discharge, i.e. $q_L > 1$;

(2) the downstream flow must be subcritical, i.e. $F_0 < 1$;

(3) the increase in sediment discharge should not exceed a critical value, i.e. $q_L < q_L^*(F_0)$, where

$$q_L^*(F_0) = \begin{cases} (4/F_0^2)^{\frac{2}{3}}; & 0 < F_0 < 0.54736, \\ 4/(\sqrt{(1+8F_0^2)}-1)^2; & 0.54736 < F_0 < 1. \end{cases}$$

When the above conditions are satisfied, the increased upstream sediment load is transported slowly downstream as a sediment bore, with speed of $O(\epsilon)$ and $O(1)$ deposition rate. However, when F_0 and q_L violate conditions (1) or (3), that is for $F_0 > 1$ or $q_L > q_L^*(F_0)$ with $F_0 < 1$, then the C_2 family of waves acquires an $O(1)$ speed but supports only an $O(\epsilon)$ step in bedform. Thus the increase in sediment load in this case is transported much faster, but with a much lower deposition rate, and a sediment bore is not formed. The sediment bore is 'washed-out' if F_0 or q_L is too large. A decrease in the upstream sediment discharge rate ($q_L < 1$) cannot lead to the formation of a discontinuous step in bedform, as all of the C_i ($i = 1, 2, 3$) waves require $q_L > 1$. It is expected that a decrease in upstream sediment discharge rate will lead to a shallow gradient expansion wave front.

Finally, a simple experiment has been performed under which conditions (1)–(3) were satisfied. Both qualitative and quantitative comparisons were made with the theory and the agreement was encouraging.

The authors are grateful to a referee for making a most valuable criticism of an earlier version of the paper.

PHILOSOPHICAL TRANSACTIONS OF THE ROYAL SOCIETY A MATHEMATICAL, PHYSICAL & ENGINEERING SCIENCES

References

Collinson, J. D. & Thompson, D. B. 1982 *Sedimentary structures*. London: Allen and Unwin

Cunge, J. A., Holly, F. M. & Verwey, A. 1981 *Practical aspects of computational river hydraulics*. London: Pitman.

Engelund, F. & Hansen, E. 1967 *A monograph on sediment transport in alluival streams*. Cophenhagen: Teknisk Vorlag.

Gibson, A. H. 1934 *Hydraulics and its applications*. London: Constable.

Hasholt, B. 1972 *Geografisk Tidsskrift* **71**, 31.

Hasholt, B. 1974 *Målinger af Materisalstransport og aflejring i Karlsgårde Sø og dens opland*. Nord Hydrologisk Konf., Aalbong.

Hasholt, B. 1977 *Grindsted-Varde Å-systemat*. Kriksølu-Undersøgeloer.

Hasholt, B. 1984 *Geografisk Tidsskrift* **84**, 10.

Jopling, A. V. 1963 *Sedimentology* **2**, 115.

Jopling, A. V. 1965 *J. Sed. Pet.* **35**, 4.

Jopling, A. V. 1977 In *Sedimentary processes: hydraulic interpretation of primary sedimentary structures* (ed. G. V. Middleton). S.E.M.P. Reprint Series 3.

King, A. C. & Bloor, M. I. G. 1987 *J. Fluid Mech.* **182**, 119.

McManus, J. 1985 Physical processes of reservoir sedimentation In *Methods of computing sedimentation in lake and reservoirs* (ed. S. Bruk). Paris: Unesco.

Nayfeh, A. H. 1981 *Introduction to perturbation techniques*. New York: Wiley Interscience Press.

Needham, D. J. 1990 *Geophys. Astrophys. Fluid Dyn.* **51**, 167.

Pitlick, J. C. & Thorne, C. R. 1987 Sediment supply, movement and storage in an unstable gravel-bed river. In *Sediment transport in gravel-bed rivers* (ed. J. C. Bathurst & R. D. Hey). London: Wiley.

Stoker, J. J. 1957 *Water waves*. New York: Interscience.

Received 26 January 1990; accepted 3 May 1990

PHILOSOPHICAL TRANSACTIONS OF THE ROYAL SOCIETY A MATHEMATICAL, PHYSICAL & ENGINEERING SCIENCES

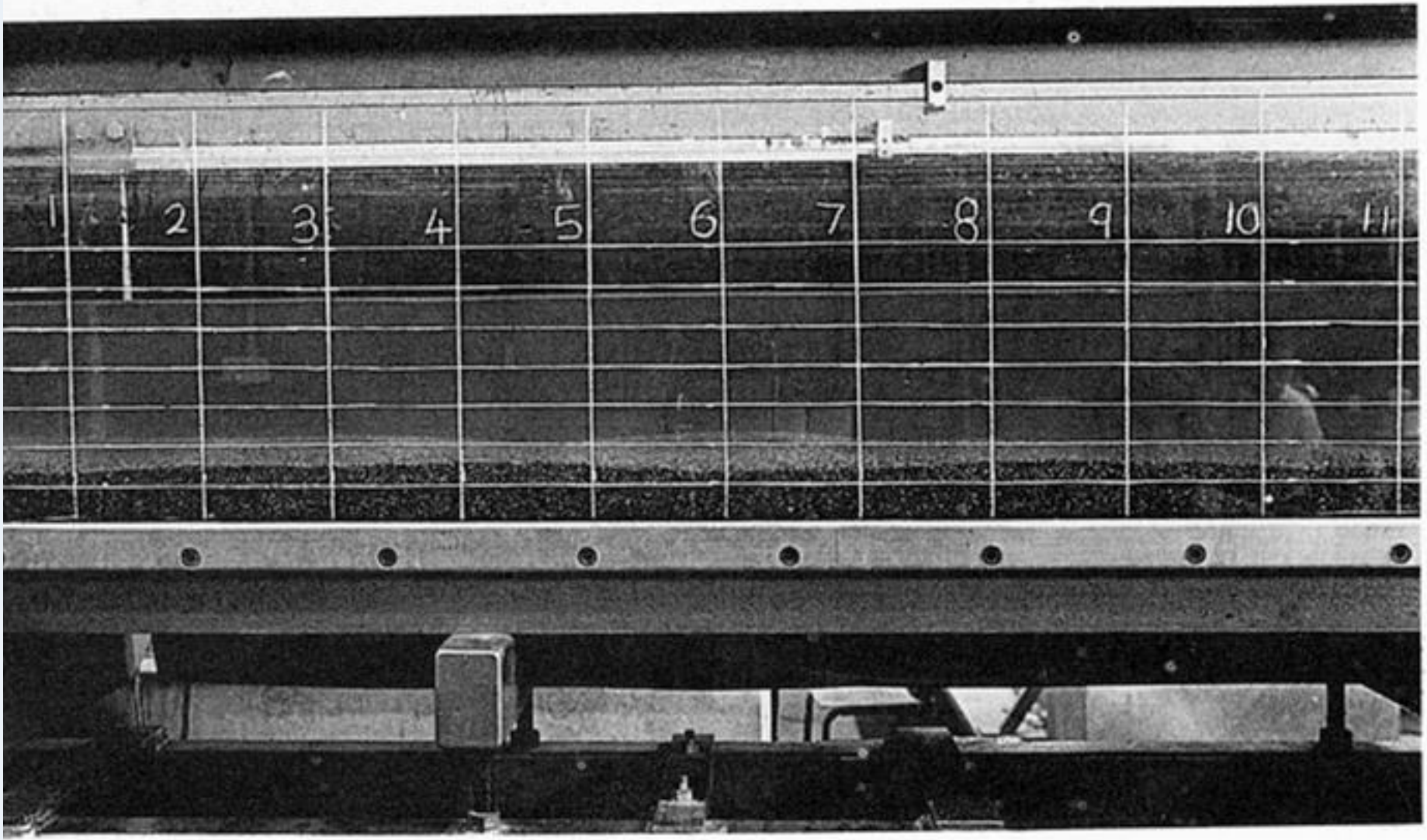

Figure 12. The uniform alluvial flow viewed through window 1.

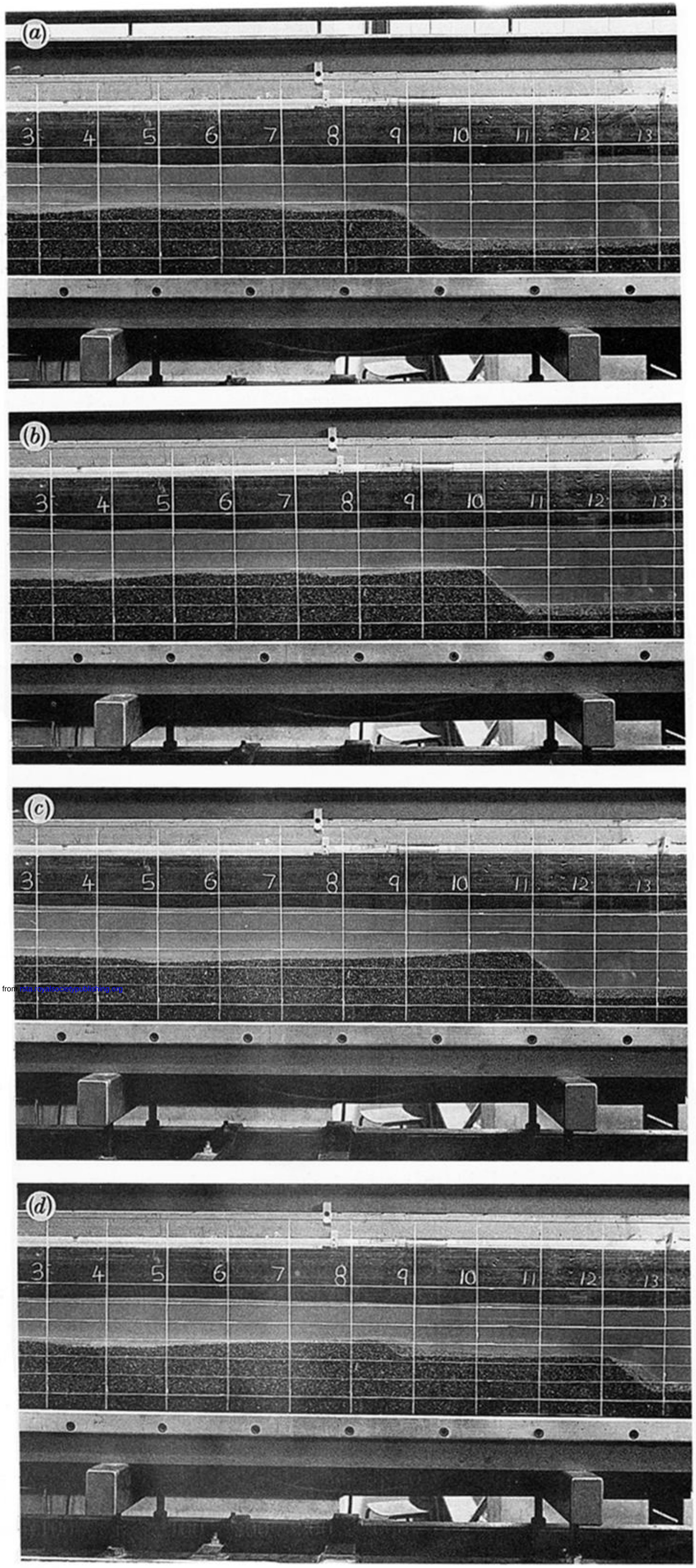

Figure 13. The transient stage in the formation of the sediment bore viewed through window 1 at times $t =$ (a) 11 min, (b) 13 min, (c) 15 min, (d) 17 min.

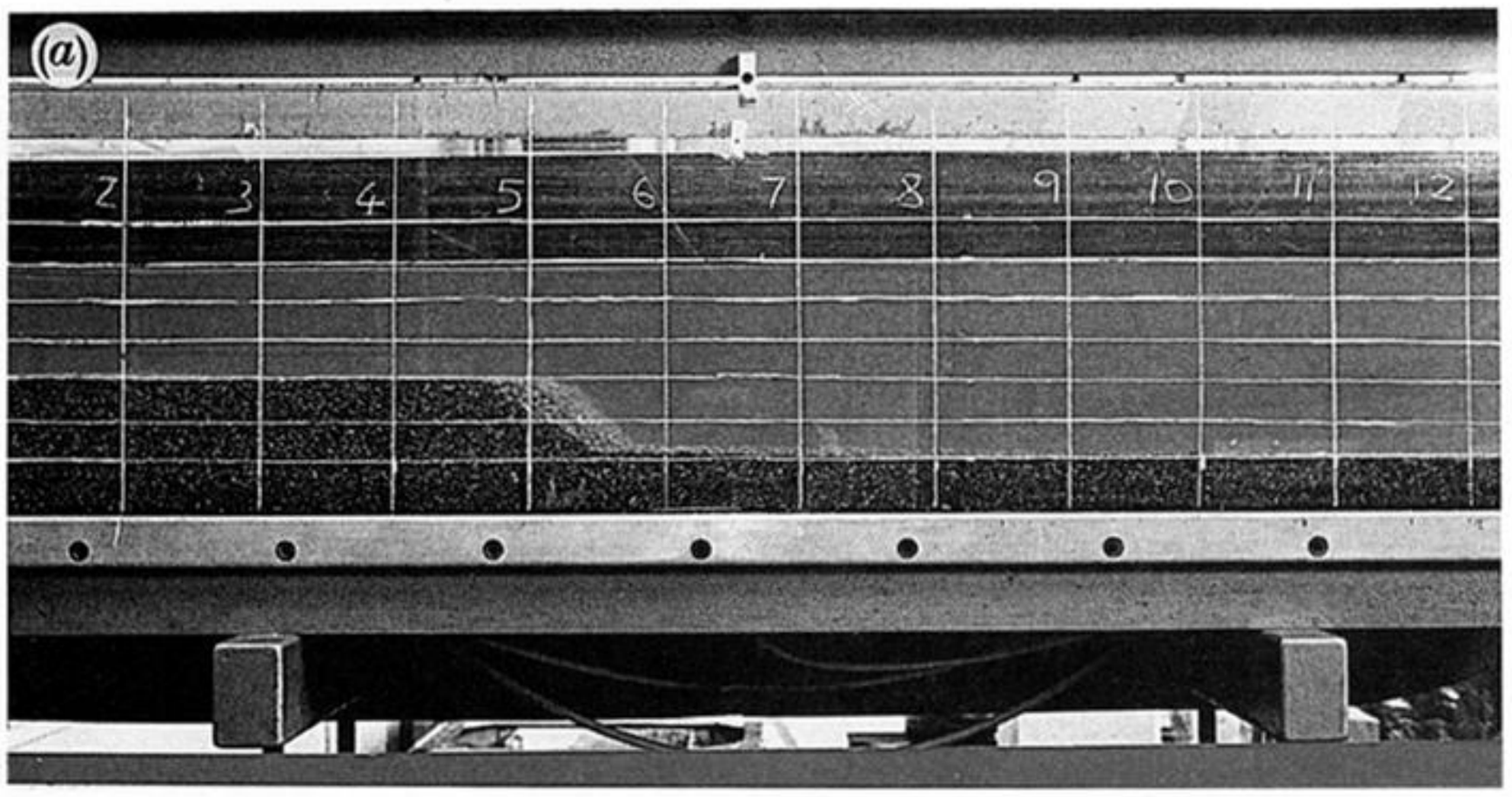

PHILOSOPHICAL TRANSACTIONS OF THE ROYAL SOCIETY A MATHEMATICAL, PHYSICAL & ENGINEERING SCIENCES

igure 14. The quasi-steady sediment bore viewed through window 2 at times $t =$ (a) 30 min, (b) 40 min, (c) 50 min, (d) 60 min. The photographs were produced in the flume at UEA.